On the validity of interface indentation technique: Experiments and Simulations

MTech. Thesis

By

JANMEJAI SHARMA

DEPARTMENT OF METALLURGY ENGINEERING AND MATERIALS SCIENCE

INDIAN INSTITUTE OF TECHNOLOGY INDORE

JUNE 2020

On the validity of interface indentation technique: Experiments and Simulations

A THESIS

Submitted in partial fulfillment of the requirements for the award of the degree

of

Master of Technology

by

JANMEJAI SHARMA

DEPARTMENT OF METALLURGY ENGINEERING AND MATERIALS SCIENCE

INDIAN INSTITUTE OF TECHNOLOGY INDORE

JUNE 2020

INDIAN INSTITUTE OF TECHNOLOGY INDORE

CANDIDATE'S DECLARATION

I hereby certify that the work which is being presented in the thesis entitled **On the validity of the interface indentation technique : Experiments and Simulations** in the partial fulfillment of the requirements for the award of the degree of **MASTER OF TECHNOLOGY IN METALLURGY ENGINEERING** and submitted in **DEPARTMENT OF METALLURGY ENGINEERING AND MATERIALS SCIENCE, Indian Institute of Technology Indore**, is an authentic record of my own work carried out during the time period from July 2018 to July 2020 under the supervision of Dr. K.Eswara Prasad, Assistant Professor, Department of Metallurgy and Material Science Engineering and Dr. Indrasen Singh, Assistant Professor, Department of Mechanical Engineering Indian Institute of Technology, Indore

The matter presented in this thesis has not been submitted by me for the award of any other degree of this or any other institute.

janmejai 17/June/2020

Signature of the student with date

(JANMEJAI SHARMA)

This is to certify that the above statement made by the candidate is correct to the best of my/our knowledge.

K. Eswara Prasad	
18/June/2020	18/June/2020
Signature of the Supervisor of	Signature of the Supervisor of
MTech. thesis #1	MTech. thesis #2
Dr. K.Eswara Prasad	**Dr. Indrasen Singh**

JANMEJAI SHARMA has successfully given his MTech. Oral Examination held on **24/June/2020**

Signature(s) of Supervisor(s) of MTech. thesis

K. Eswara Prasad

26/June/2020

Convener, DPGC (Date)

Dr. Mrigendra Dubey

Signature of PSPC Member 1	Signature of PSPC Member 2
Dr. Hemant Borkar	**Dr. Sumanta Samal**
	S. Samal

ACKNOWLDGEMENTS

It is a well-known fact that no matter how big or small the work is, it takes effort to get it to fruition. During this quest of project there are many people who are like steppingstones in the way to success. Their support is undeniably crucial, and I am grateful to have support of such great people during my research work.

To begin with, I would like to convey my sincere regards to my mentors Dr. Eswara Prasad Korimilli and Dr. Indrasen Singh for providing their support and guidance during this entire journey of research work. Dr. Eswara not only acted as guide to carry out the work but also provided a crucial support be it technically or emotionally. The congenial personality of both Dr. Eswara and Dr. Indrasen was an asset to have for this work done efficiently. Despite being a person of tremendous technical acumen, Dr. Indrasen was always available to have vital discussions, which not only helped me to gain technical knowledge but also it taught me various life skills. Therefore, I offer my regards to my mentors for being with me.

I am also grateful to Dr. CP Paul and Dr. AK Rai of *Raja Ramanna Centre for Advanced Technology (RRCAT), Indore* for granting me access to the micro-hardness testing facility. For conducting these experiments, I want to express my gratitude to Mr. Sunil Kumar Yadav (RRCAT) for helping me out in this regard. I would also like to thank Dr.Venkat A N Ch of *Advanced Materials and process research institute (AMPRI), Bhopal* for providing access to the rolling mill at their facility.

I would like to express my indebtedness to the PSPC members Dr. Hemant Borkar and Dr. Sumanta Samal for providing their crucial insights in assessment of this work during the research work.

I am obliged to Dr. Vinod Kumar, Head of Department- MEMS for providing all the technical and official support required to carry out the project efficiently and successfully.

I am also thankful to my lab mates Mr. Abhinav Sharma, Ms. Tulika Dixit, Mr. Sheetal, Mr. Vaibhav Kathavate, Mr.Hirmukhe and Mr. Chaitanya Vishwakarma for their help during this journey.

I want to express my thanks to lab technicians Mr. Mayur Dhake And Mr. Deepak Rathore for aiding me in lab work.

I want to thank my friends Anurag Sharma and Nilay Upadhyayfor providing help me in completion of the thesis work.

I am thankful to my friends and classmates at IIT Indore for their support and help.

Lastly, I am thankful to my family for their support and IIT Indore for giving me such an experience of lifetime.

DEDICATION

I would like to dedicate this work to my mother Late Mrs. Sushma Sharma and to my family, friends and almighty god.

SYNOPSIS

Indentation is an extremely useful tool to indirectly estimate the strength of materials for nearly a century now since the invention of Brinell method. Though it is confined to indirect measurement of strength till few decades, the advent of "instrumented indentation" made it possible to obtain the elastic properties like elastic modulus but still elusive to determine the characteristic properties like yield strength, ductility, and work hardening exponent which requires a comprehensive understanding of deformation zone underneath the indentation. The experimental determination of subsurface deformation zone by plastic strain mapping proposed by Chaudhri and co-workers is extremely time consuming (because of the several steps involved in it) and sometime may not even possible to perform on brittle materials like ceramics, bulk metallic glasses etc. Interface indentation experiments can be an alternative to this as they are relatively easy to perform on all classes of materials. A large number of these experiments is performed in recent years on bulk metallic glasses also reveals the deformation mechanism which otherwise not possible by conventional constrained indentation experiments. However, there is no validation of the interface indentation experiments barring few early experimental studies by Mullhearn, Tabor, and others who has shown that the plastic zone shape of interface indentation samples is like the conventional ones. Again, there are no systematic investigations clearly describing the role of interface width, state of the material (annealed or work hardened) on the shape and size of the plastic zone. In this work, the subsurface deformation zones of constrained and interface indentation samples under a spherical indentation is investigated. Further the hardness mapping is used to compare the differences in deformation zone size in the work hardened samples. Finite element simulations are performed to understand the shape and size of deformation zone and compared with the experiments. Oxygen-free high-conductivity (OFHC) copper is used in the experiments as it is too easy generate a range of strain hardening exponents by changing the deformation history in these samples. In addition to this OFHC an attractive model material as a wealth of information is available regarding constitutive modelling, microstructure response, mechanical properties and sensitivity to strain hardening to assess the plastic strains.

Table of Contents

List of Figures

List of Tables

1.INTRODUCTION

The term hardness has several definitions associated to it. For metals, it is defined as a resistance to permanent deformation. From a metallurgist's point of view, it means resistance to penetration. From tribological and surface engineering perspective, it means resistance to wear. From a design engineer's point of view, it is a quantification of measure of flow stress. For a mineralogist, it is the resistance to scratching, and to a machinist, it means resistance to machining in relation to tool wear. Hardness can correspondingly be mentioned to as mean contact pressure. Hardness, as functional to most materials and metals, is a valuable parameter in revealing the mechanical properties and is an often-employed mechanical test, that has been in use in for more than a century. Undoubtedly, as a material property, the value and importance of cannot be understated, the information obtained from a hardness test can complement and often be used in concurrence with various other material corroboration practices such as tensile or compression tests to provide critical design insights. The reputation of the hardness testing has covered various facets of engineering domains which includes the likes of structural, aerospace, automotive, quality control, failure analysis and countless other forms of manufacturing industry. Determination of these material properties provide a valuable perception to the durability, strength, flexibility, and proficiencies of a variety of component types extending from raw materials to finished specimens and goods. Over the years, various methods for shaping the hardness of materials have been developed and employed at many levels. From early forms of scratch test to sophisticated automated imaging, hardness testing has transformed into an efficient, accurate and important material testing method.

In recent years testing procedures and hardware have significantly enhanced, because of the rapid advancement in the fields of electronics, computer hardware and programming etc. Elementary forms of hardness testing in earlier days comprised of a simple scratch test. The roots of the most basic forms of hardness testing was bar scratch testing which dates to 1722. These tests were created to scratching a bar with increased hardness from end to end. Later, in 1822, hardness testing methods were introduced which included scratching the material surfaces with a diamond and measuring the width of the resultant line, this test later came to be known as the Mohs scale.

The Mohs scale was one of its kind of testing method available at that time thus it pioneered its way in hardness testing scenarios because of its concept relative and graded measurement, in some processes this method is still utilized today for e.g. in assessment of scratch resistance of mobile screens.

The Mohs scale comprises of ten minerals which are ordered from hardest at 10 (diamond) to softest at 1 (talc). Each mineral can scratch those who fall below it in the scale grading. The Mohs scale is not linear and thus the change in hardness of materials between 9 and 10 is significantly more than that of those between 1 and 2, an example explaining this scenario is hardened tool steel which is at approximately 7 or 8 on the scale. During the next 75 years, more refined versions of the scratch test were introduced which included integrated microscope, stage and a diamond apparatus which applied loads up to 3 grams as a setup. The material to be tested was scratched under the variation of load and further subjected to comparison to the standard set of scratches of known value. A more advanced version of this system employed a diamond mounted at the end of a tapered steel spring, the other end of the spring was connected to a balancing arm with a 3-gram weight. The material under test was moved by a hand actuated wheel and a worm gear system. On top of it there was a stage and a holding fixture for the material. The pressure was applied, and the material was traversed thus resulting in a "cut" in the material. This cut was then observed and measured under a microscope with the aid of filar micrometer eyepiece.

Indentation type of hardness testing in the early stages was developed around 1859. It was based on the concept of magnitude of load essential to produce an indent of 3.5 mm in the material. The depth of the indentation so obtained was then measured with a Vernier scale and the total load required to reach the 3.5 mm was termed as the hardness. The penetrator/indenter contained a truncated cone with a geometry in the form of a taper of 5 mm at the top and 1.25 mm at the point. This method had a flaw that it was mostly effective for soft materials. Another early form of indentation test involved pressing a right-angled geometry of the similar test material onto one another and thereby gauging the width of the resultant impression. Various systems advanced from this practice during the early 1900's that also utilized "mutual" indentation of cylindrical test material with the longitudinal axis pressed at right angles to one another.

1.1 Types of hardness evaluation methods

a) Brinell Hardness Testing

The first extensively recognized and consistent indentation-hardness assessment was proposed by J. A. Brinell in 1900. Brinell's curiosity in materials grew during his participation in a several Swedish iron making and fabrication companies which led to his desire to have a consistent and rapid means for determination of material hardness. The Brinell hardness test, a broadly used method, comprises of indenting the metal surface with a 1 to 10 mm diameter steel or a tungsten carbide ball at heavy loads of up to 3,000 kg. The resultant impression diameter of the indentation is measured under a microscope after removal of the load. The average of two readings of the diameter of the impression at right angles is taken and further calculation is done to get a hardness value using a mathematical formula. The Brinell hardness testing pioneered the way for indentation hardness testing and paved the way for indentation tests that were more relevant to material types. One of the limitations of BH tests is its inability to apply for hard materials due to the limitations of the indenter material. The Brinell hardness number (BHN) incorporates the actual area of the curved surface of the impression so BHN is given as $\mathrm{BHN} = \frac{2P}{\pi D\,(D-\sqrt{D^2-d^2})}$

- P is the applied load (kgf)
- D is the diameter of the indenter (mm)
- d is the diameter of the impression (mm)

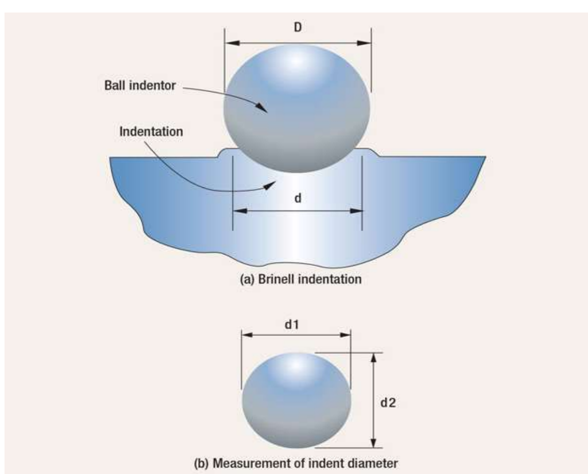

Fig.1. 1 Brinell Indentation [1]

(b) Vickers and Knoop Hardness Testing

A substitute to the Brinell hardness testing, Vickers hardness test was established in 1924 by Smith and Sandland, at Vickers Limited, a British Engineering corporation. The test was envisioned in response to the necessity of a more advanced test over the Brinell hardness test as it has material limitations. The Vickers test works on an identical principle as that of Brinell, it also requires a measured impression on the material, but instead of spherical indenter it used a pyramid shaped diamond. Because of this a more consistent and versatile hardness test was developed. Later, in 1939, a substitute to the Vickers test was given by Fredrick Knoop at the US National Bureau of Standards. The Knoop test employed a shallower and elongated form of the diamond pyramid indenter. It was designed for the use of lower test forces than the Vickers hardness test, allowing for more accurate testing of brittle or thin materials. Knoop test is also a vital tool in assessment of anisotropy in materials. Both the Vickers and Knoop tests are still considered amongst the popular hardness analysis methods today. The Vickers hardness test method consists of indenting the test material with a diamond indenter, in the form of a right pyramid with a square base and with an angle of 136 degrees between opposite faces (Fig.1.2) subjected to a load in the range of 1 to100 kgf. The load is usually applied for 10 to 15 seconds. The two diagonals of the indentation left (Fig.1.3) in the surface of the material after removal of the load are then measured using a microscope and their average is calculated. The area of the sloping surface of the indentation is calculated using a formula mentioned below.

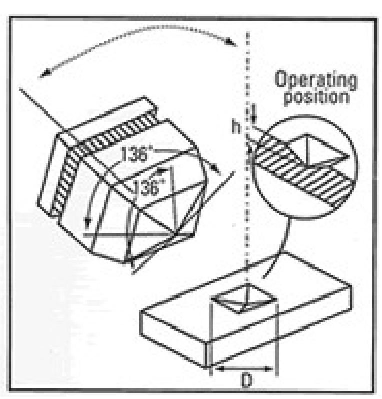

Fig.1. 2 Vickers Indenter [2]

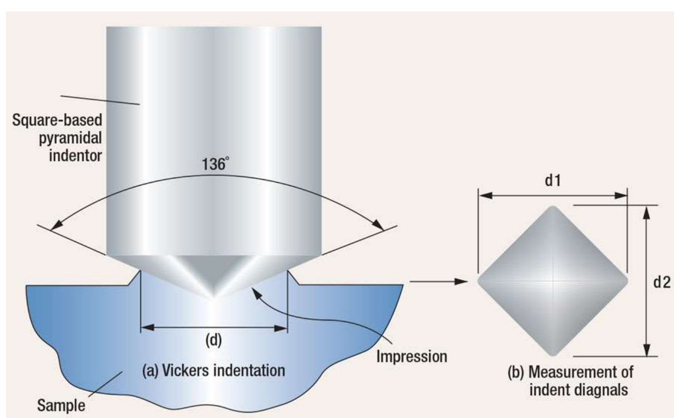

Fig.1.3 Vickers Indentation [1]

$$\text{Vickers Hardness (HV)}=\frac{2P}{d^2} sin\frac{136°}{2} =1.854\frac{P}{d^2}$$

Where P is the applied load (kgf) and d is the mean diagonal of the indentation (mm).

The diamond indenter employed in the Knoop testing has a shape in the form of an elongated four-sided pyramid. The angle between two opposite faces being nearly 170° and the angle between the other two being 130° (Fig.1.4 and 1.5). The indenter is pressed into the material under loads that are often less than 1 kgf, the indenter carves a four-sided impression about 0.01 to 0.1 mm in size. The length of the impression so obtained is approximately seven times the width, and the depth is 1/30 of the length. Given such dimensions, the projected area of the impression under the load can be calculated after measuring the length of the longest side with the help of a calibrated microscope. The final Knoop hardness (HK) is derived from the following formula.

$$\text{HK}=\frac{2P}{d^2\left[\cot\frac{172.5}{2} tan\frac{130}{2}\right]} = 14.24\frac{P}{d^2}$$

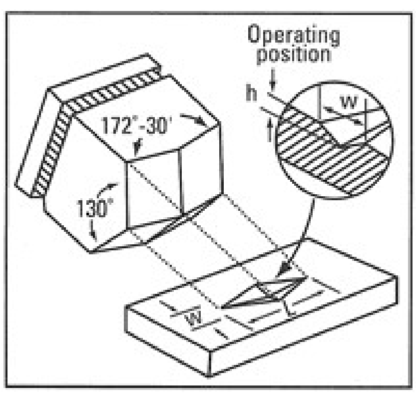

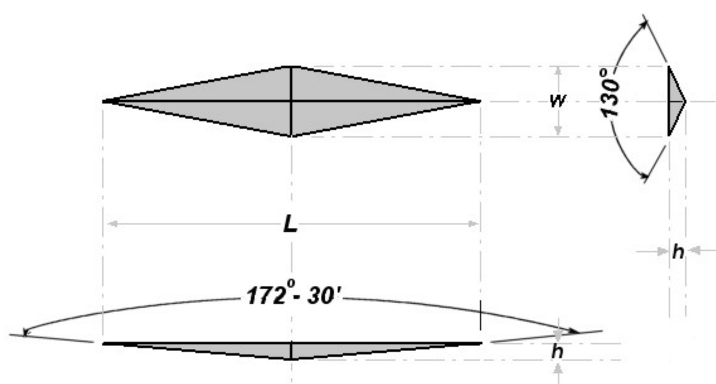

Fig.1.3 Knoop Indenter [2]

Fig.1.4 Knoop Indenter top view [3]

(c). Rockwell Hardness testing

The Rockwell Hardness Test is generally a non-destructive test. Hugh M. Rockwell (1890–1957) and Stanley P. Rockwell (1886–1940) from Connecticut co-invented the first tester and got its patent granted in 1919. The Rockwell Hardness test is commonly considered as easier to perform in contrast to methods like Vickers and Brinell. The Rockwell hardness testing involves indenting the test specimen with a diamond cone or hardened steel ball indenter. The test is performed using two loads applied to the sample. First, the indenter is enforced into the test material under a preliminary minor load and the depth so formed is recorded. With the minor load still applied, an additional load is introduced which is the major load and it increases with the depth of penetration on the sample. The major load is then removed, and the force on the sample is returns to the minor load. Subsequently, the increase in the depth of penetration which is obtained from the application and removal of the major load is used to calculate the Rockwell hardness value (Fig.1.6).

Rockwell or Superficial Rockwell depends on the material under testing. Both utilize the HR scales. Indentation on the Rockwell testing machine is performed with either a diamond core (HRC) or a hardened (tungsten) steel-ball indenter (HRB). By applying a preload of 10 kgf which is followed by a main test force of 60, 100 or 150 kgf, a penetration is done, and size of the impression is measured. For brittle or very thin materials (e.g., thin strip or lightly carburized surfaces, small parts or parts that might not hold up under a standard Rockwell test), then Superficial Rockwell scales are recommended as they use lower force and produce shallower impressions. It explicitly use a 3 kgf preload and main test force of 15, 30 or 45 kgf.

Rockwell test samples are classified on the basis of HR scale given in Table 1.1 : A (cemented carbides, thin steel, shallow case-hardened steel); B (copper alloys, soft steels, aluminum alloys, malleable iron); C (steel, hard cast irons, pearlitic malleable iron, titanium, deep case-hardened steel, plus other materials harder than B); D (thin steel and medium case-hardened steel, pearlitic malleable iron); E (cast iron, aluminum, magnesium alloys, bearing metals); F (annealed copper alloys, thin or soft sheet metals); G (phosphor bronze, beryllium copper, malleable irons); H (aluminum, zinc, lead); and K, L, M, P, R, S and V (bearing metals, plus other very soft or thin materials).

Table 1 Rockwell HR scale [2]

SCALE	NAME	INDENTER	LOAD (kN)
A	HRA	120º diamond spheroconical	0.588
B	HRB	1/16″ steel sphere	0.980
C	HRC	120º diamond spheroconical	1.470
D	HRD	120º diamond spheroconical	0.980
E	HRE	1/8″ steel sphere	0.980
F	HRF	1/16″ steel sphere	0.588
G	HRG	1/16″ steel sphere	1.470

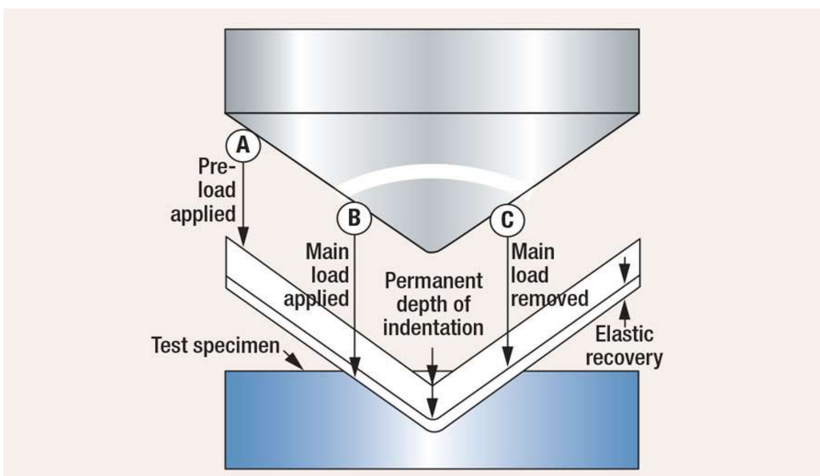

Fig.1. 5 Rockwell Indentation [1]

1.2 Advances in hardness testing methods: Instrumented indentation

Characterization of deformation field beneath the indentation is of utmost importance for understanding the mechanics of indentation testing and many industrial deformation processing methods like forging, extrusion, machining and shot peening etc. which operate on similar principles. Further, this particularly useful in understanding inverse problems where it is possible to extract the uniaxial parameter from simple indentation tests. There have been significant number of studies since 1940's to understand indentation problems and with the development of computation capabilities. Therefore, the deformation field underneath indentation has been a subject of renewed attention with the development of strain gradient plasticity models, analytical solutions and microstructural studies for which accurate measurements of such fields are decisive in determining the flow behavior of material beneath the indenter. Recent developments in experimental techniques such instrumented Nano/micro indentation has helped in estimating the material's properties such as elastic modulus and to some extent the fracture toughness. However, understanding the uniaxial properties such as yield strength, strain hardening exponent and ultimate tensile strength is far from complete. This is due to the complex material's plastic flow behavior under the indenter which often results in pile-up or sink-in behavior. In such cases, the elastic modulus obtained from analytical solutions is over or underestimated. An improved understanding of the plastic flow, by both experiments and complementary simulations, underneath the indenter will be helpful in accurately estimating the mechanical properties However, understanding the uniaxial properties such as yield strength, strain hardening exponent and ultimate tensile strength is far from complete. This is due to the complex material's plastic flow behavior under the indenter which often results in pile-up or sink-in behavior. In such cases, the elastic modulus obtained from analytical solutions is over or underestimated. An improved understanding of the plastic flow, by both experiments and complementary simulations, underneath the indenter will be helpful in accurately estimating the mechanical properties.

Monumental improvements have been done in recent years in hardness testing. This is possible due to the development taken place in the fields of instrumentation, computer hardware, electronics, imaging algorithms, and software capabilities. This has led to an extremely precise and reliable testing methods which provide results more quickly than ever before, often in automated manner. These components and techniques have proven to be beneficial in raising efficiency, speed, and accuracy to an unmatched level. Over the past several years more traditional manual test processes have paved the way to automation in every aspect of the testing process.

New practices in sample preparation, handling, mount fixturing, stage movement, results interpretation and analysis have now been introduced to the hardness testing industry. One such recent outcome of the advancement of the technology as mentioned above is Instrumented indentation testing also known as the nanoindentation testing. The nanoindentation testing is simply a refined version that has length scale of penetration in nanometers $(10^{-9}m)$ rather than millimeters $(10^{-3}m)$ which a characteristic feature in macro hardness tests. In conventional indentation, the area of contact is calculated from direct measurements of the dimensions of the residual impressions created by the indentation load. In the nanoindentation since the scale is in the orders of nanometers, therefore the measurement of area of the impression becomes a tedious task. Thus, to determine the area of contact, depth of penetration of the indenter into the specimen is measured. This, together with the known geometry of the indenter provides an indirect measurement of the contact area at full load. Because of this reason nano indentation is also referred to as depth sensing indentation (DSI). For such measurements to be made, the depth measurement system needs to be referenced with the specimen surface.

This is usually done by keeping the indenter in contact with the surface with a very small contact force leading to a small penetration into the surface of test specimen.

Various modifications are required to be taken into consideration for anomalies associated due to shape of the indenter, deflection of the loading frame and history of the material. As these anomalies can lead to an error in recording the depth of the penetration which can eventually lead to an error in the values of hardness and elastic modulus of the specimen.

The nanoindentation test can give an information about the elastic modulus, hardness, strain hardening, cracking, phase transformations, creep and energy absorption of the test specimen. Since the sample size is very small, the testing can be nearly considered as a non-destructive type. As the deformation scale is so small, the technique is readily utilized the analysis of thin surface films and surface modified layers. In many cases it has been found that the microstructural features of a thin film or a coating differs from the bulk material due to the presence of residual stresses and difference in the morphology of the structures. Hence in order to assess the variation in properties associated with difference in the coating and substrate material, nano indentation is a useful tool.During the nanoindentation testing an indenter is pressed against a flat specimen surface with increasing load steadily. Both load and depth of penetration are recorded at each load increment which provides a measure of modulus of elasticity and hardness as a function of depth beneath the surface. Furthermore, after the maximum load is attained, the load is steadily removed, and penetration depth is recorded. The loading part of the curve may consist of an initial elastic contact, followed by plastic flow or yield at higher loads. Upon unloading, if yield has occurred, the load-displacement curve follows a different path until at zero applied load and a residual impression is left in the specimen surface. The maximum depth of penetration at a given load along with the slope of the unloading curve measured as the tangent to the data point gives the value of hardness and young's modulus of the material.

In some cases, it also possible to get the elastic modulus in loading portion of the curve. For a viscoelastic material, the relationship between the load and the depth of penetration is peculiar that is for a given load, the resulting depth of penetration may depend on the rate of application of load as well the magnitude of the load. For such materials the indentation test is accompanied by creep (Fig.1.6). The analysis of this creep portion reveals an information about the material like it has elastic "solid like properties" of the specimen and also the "liquid like or out of phase" components of the specimen present. In case of brittle materials, cracking may occur specifically when using a pyramidal indenter such as three-sided Berkovich Indenter or a four-sided Vickers indenter (Fig.1.7). As shown in figure (Fig.1.8) the length of the crack, which often begins at the corners of the indentation impression. The assessment of this crack propagation can used for calculation of the fracture toughness of the material. As these P *vs*. h curves are very sensitive to the underlying deformation zone, it is very important to understand the plastic strain distribution underneath the indentation.

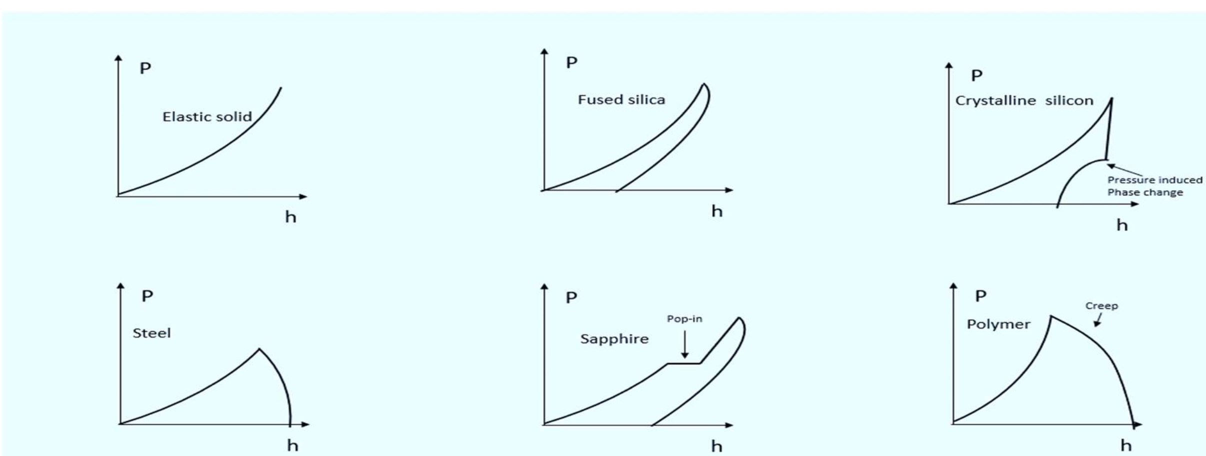

Fig.1.6 Schematic load-displacement curves

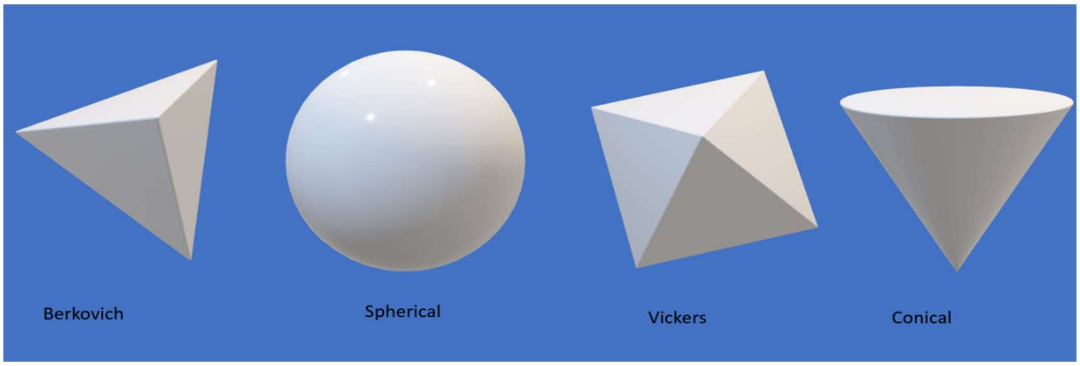

Fig.1.7 Types of indenter geometries

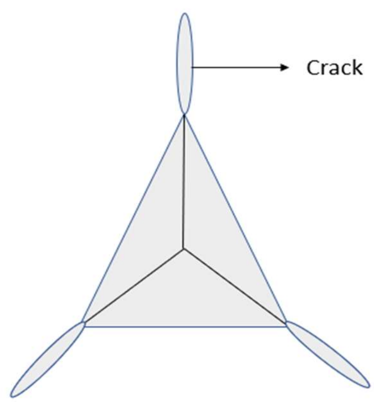

Fig.1.8 Cracks emanating from the corners of a brittle material after indentation

1.3 Plastic strain distribution beneath the indentation

The plastic strain or representative strain plays an important role in the field of contact mechanics of elastoplastic solid and indentation experiment is one such case. Tabor (1948)[3] is one of the pioneers in this regard who gave the term "representative strain". He defined it as the total indentation strain imposed by a spherical indenter as ε_r= d/D where d is the diameter of the impression and D is the diameter of the indenter. The study included the construction of stress-strain curves, which were dependent on the fact that impression diameter (d) increases with increase in applied indentation load. The results so obtained differ from the usual compression stress-strain curve by a factor of 2.8.

The corresponding strain values so obtained were in the range of 8-10% for a Vickers indentation, moreover strains were found to be independent of the size of the Vickers indenter.

In 1957 Samuels and Mulhern [4] did an investigation of deformed zone beneath a spherical and conical indenter. The purpose of this work was to determine the shape and size of the deformation zone using distortion markings .The key observations they got was that in both the indenters the plastic strain distribution and deformation zone appeared to be in the shape of a hemisphere the extent of deformation or size of deformation was supposed to 2.1 times the impression diameters for spherical indenter and 1.7 times the impression diagonal for the conical indenter. The representative strains so obtained for ball or spherical indenter was around 10% and for the conical indenter it was around 8% which was in correspondence with Tabors (1948) work.

In 1958 a year later Mulhern [5] conducted a bonded interface experiment using cold work carbon steel specimen in order to assess the nature of the deformation zone using distortion grid engravings. These engravings served the purpose of gauging the strain contours formed due to indentation. Consequently, the shape of the contour so obtained was in accordance with the previous Samuels and Mulhern study which resembled to a hemisphere. Later in 1965 Atkins and Tabor[3] did conical indentations on copper and steel samples by varying the indenter geometry to find the indentation strain or representative strain (ε_r) which is termed as ;due to the indentation, the material beneath it undergoes severe plastic deformation. Because of this a complex state of strain field is generated which changes from point to point. Since the deformation is of plastic behavior, the corresponding strain values are more than the yield strain of the material. Thus, the indentation strain is the difference of strain after indentation and yield strain of the material. This led Johnson in 1970 [6] to purpose a model for material deformation beneath the indentation. Also, the study led to a proposition for representative strain for a Vickers indenter, which is given as ε_r= 0.2 $Cot\ \alpha$ where α is the angle of the indenter. The values of strain were in the range ~8% in correspondence to Atkins and Tabor's work.

Chaudhri in 1996 [7] conducted sub surface indentations experiments and suggested that Tabor's model is invalid for the power law hardening solids. The study also disregarded the shape of strain profiles proposed by Samuels and Mulhern in 1957 is proposed that shape of the deformed zone is more elongated along the loading axis and it doesn't appear like a hemisphere for ductile materials. In 2011 Prasad et.al. [8] utilized Chaudhri's work [7] and carried out a similar sub surface mapping technique and studied the plastic strain distribution and shape of the deformation zone underneath conical indenters of different geometry. A comparative study of experiments and finite element simulation was done. This led to a proposition that the nature of the elastic plastic boundary is of elliptical nature which contradicted the hemisphere nature of the boundary.

1.4 Interface indentation technique

The bonded interface technique or experiment is a one of its kind approaches utilized to assess the deformation characteristic features associated with an indentation testing experiment. For the past 70 years indentation is one of the most sought-after topics for researchers and various research studies have been done so far in order to understand the peculiarities related to the complex nature of stress and strains beneath an indentation experiment. Initially it may appear that an indentation experiment is just a scenario of simple compression testing as per the definition, but in actual sense it is far more intricate in comparison to it. The tri-axiality of stresses and strains along with the hardening of materials cause the behavior to change drastically.

The first ones to employ the bonded interface experiments was Mulhern (Fig.1.9) in 1957 [4]. It was named as the composite block technique. It involved two split samples in the shape of rectangular prism with top, side and bottom surfaces polished to mirror finish. Subsequently, the samples were engraved with square grids of size 0.5mm on the faces which were to be joined. The joining was done using bolts. The objective of the whole experiment was to gauge the extent and shape of the deformation zone associated with an indentation experiment. The moto of this study was that whenever a material is indented, the deformation extends beneath the material surface hidden and surrounded by material. Thus, in order to visualize and gauge the true nature of indentation the sample is sectioned off from the center of the indented impression which is usually followed by metallographic treatments and microscopic characterization. But it is a highly likely scenario that during cutting along the indent, regardless of the fineness of the cut, the true nature of the of deformation seems to get affected. Therefore, the bonded interface method comes into picture.

Another way of getting the bonding between the samples is by using Cyanoacrylate glue or super glue for the joining of the specimens (Fig.1.10). This is usually followed by an indentation at the center of the junction. The benefit of this approach is that it is not only confined to a single set of materials like metals but also can be employed to ceramics [9] and Bulk metallic glasses [10]too.

Despite all these benefits a key issue associate with this is the strength and integrity of the bonded interface. As during indentation, the loads so applied can is usually for a duration of 20s to 30s and during this time the strength should be adequate to withstand the applied load. Another issues with the bonded interface indentations is the relaxation of stresses due to the compliant interface

Recently bonded interface technique has got the attention of the researchers and various studies have been conducted so far. Zhang et.al [11] utilized this method in assessment of the deformation zone beneath Vickers indenter for Zr-Hf based bulk metallic glass (BMG). The proposition that came out of this study is that in bulk metallic glasses the deformations occur in the form of slip steps beneath the indenter (Fig.1.11a). Similarly, Subhash and co-workers carried out static and dynamic indentation experiments [12] on Zr-Cu based BMGs on cylindrical split specimens (Fig.1.11b). The study aided them to observe the shear band patterns under static indentation, dynamic indentation and dynamic scratch respectively in BMGs. They concluded that spacing of shear bands is more severe in dynamic indentation in comparison to static one. Also, the effect of change in indenter geometry to ball indentation has lead observation of spiral shear bands in a bonded interface specimen.

The bonded interface indentation method has also made its way in the field of biomedical applications in 2005 Imbeni et. al [13]conducted interface indentation at dental enamel junction in order understand the fracture toughness and crack propagation characteristics of the dental enamel junction of the human teeth. Thus, bonded interface technique has shown its prominence in assessment of deformation behavior of different materials beneath the indention. Therefore, in our study we have incorporated it to understand the behavior for Oxygen free high conductivity (OFHC) copper.

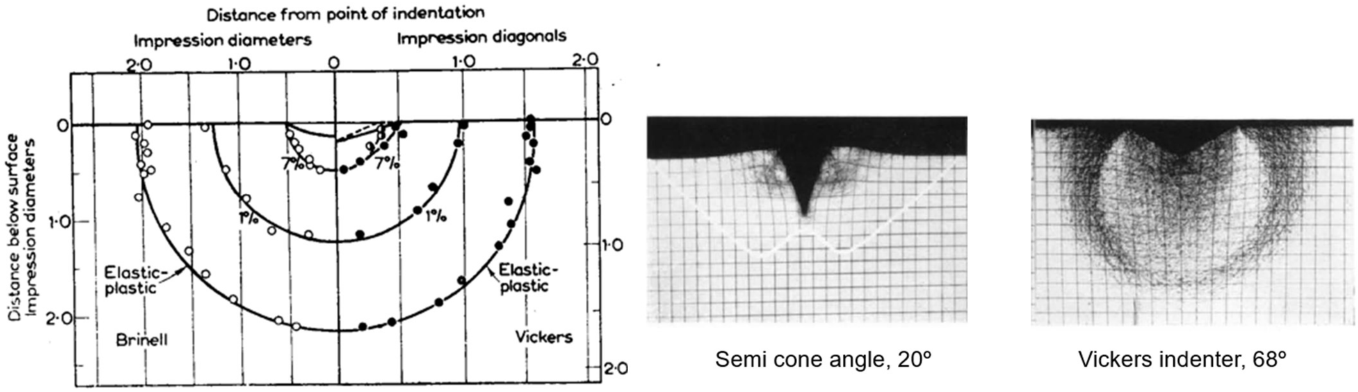

Fig.1.9 Bonded interface results of T.O Mulhern [6]

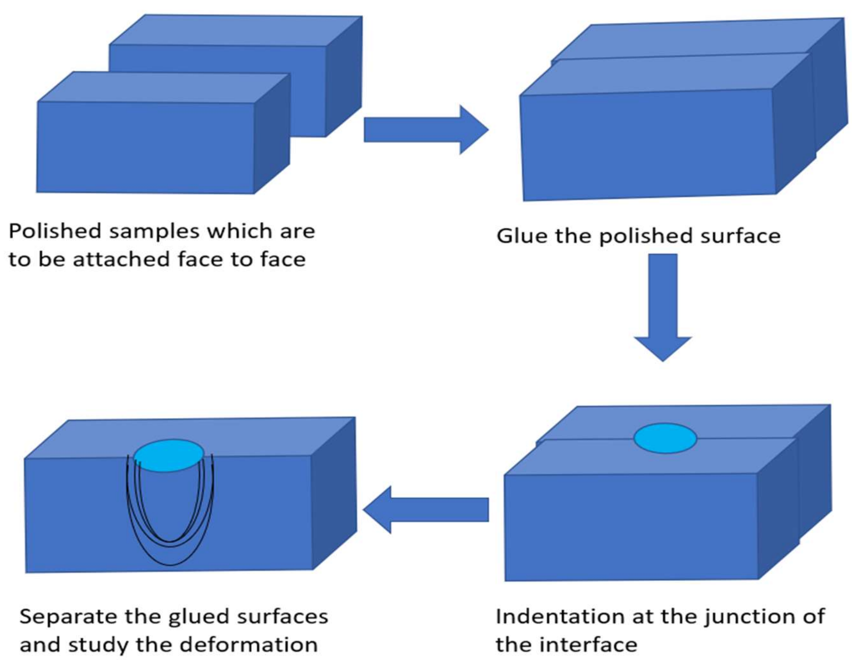

Fig.1. 10 Bonded Interface technique using super glue

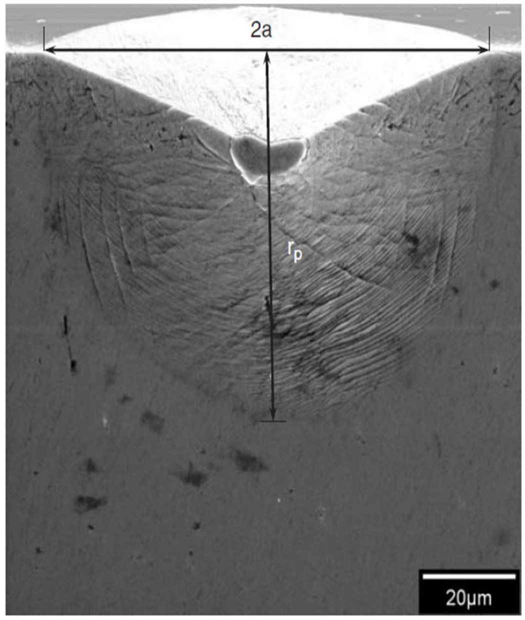

a) Vickers Indentation on Zr-Hf based bulk metallic glass [11]

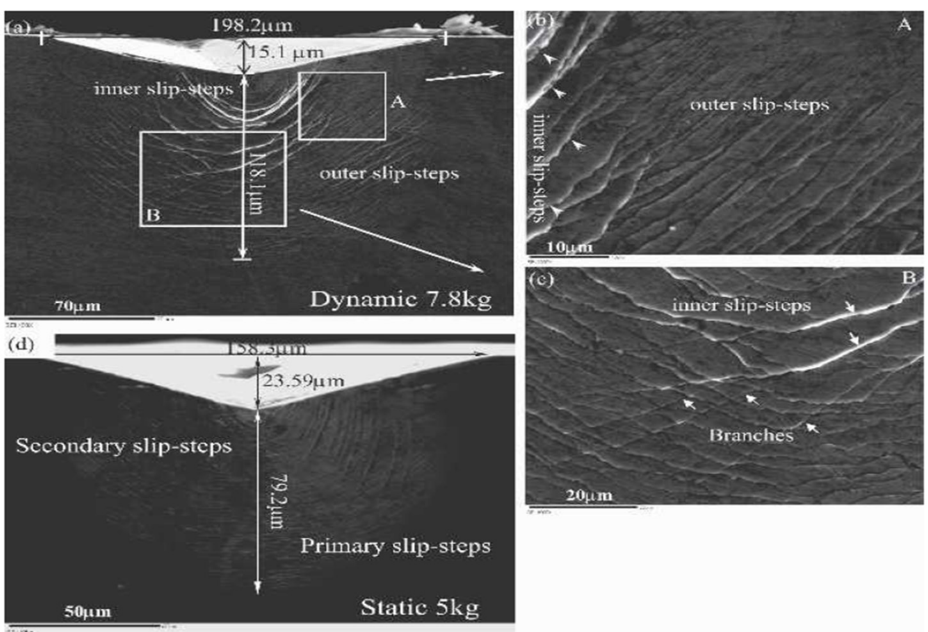

b) Dynamic and static indentation on Zr-Hf based bulk metallic glass [12]

Fig.1. 11 Bonded interface slips patterns in bulk metallic glasses (a & b)

2.LITRETURE REVIEW

A large number of research studies have been carried out on the behavior of material beneath the indenter. Almost 80 years of studies have been done so far in this regard. One such attempt is being made in our current study. A review is done in order to ascertain various works done involving experimental and simulation-based investigation of indentation carried out on different materials with varying geometries of the indenters.

To begin with Hill et al.[14] were amongst the first to investigate the plastic flow response of Cu and Pb samples. The indentation was carried out using different wedge indenters with varying the semi-angle α between 7º and 30º. Their study led to a proposition that the plastic flow underneath a sharp indenter is of "cutting nature". Consequently, Hill proposed the slip-line filed theory, which states that the material underneath the indenter gets displaced sideways and upwards from the face of the wedge indenter. The validation of the slip-line filed theory was done by Dugdale[15] . During his work Dugdale performed wedge indentations on various cold worked samples. Later, one of the monumental works was done by Samuels and Mulhern [4]. They utilized the differential etching ability of 70:30 brass to examine the plastic flow under spherical and Vickers indentation. This led to a finding that the material beneath the indenter flows radially outwards and shape of the elastic-plastic boundary is of hemispherical shape. Later, Mulhern [5] carried out the bonded interface experiments subjected to indentation on a highly work hardened steel and found that the plastic flow occurs via cutting mechanism under a sharp indenter ($\alpha = 20°$) whereas it is of radially compressive nature for blunt indenters like Vickers.

Dugdale carried out Vickers indentations on different materials and concluded the spherical cavity model cannot directly suffice for the hemispherical nature of the deformation, as the mean pressure required expand the cavity is almost twice of that of required for a shallow indent. Marsh [16] conducted the Vickers indentations on glass and suggested that mean pressure predicted by spherical cavity model do not comply to the experiments. Similar observation was made by Hirst and Howse [17], who studied wedge indentation experiments on different metals and made a proposition to the spherical cavity model that certain modifications had to be made like introducing the parameters like E/Y to describe the compressive flow mechanism associated with indentation.

Atkins and Tabor [3] conveniently studied the indentation response of Cu and mild steel using conical indenters pf different geometry with varying the semi-angle from 30º to 75° and found that at 52.5º the mechanism of indentation changes from cutting to radially compressive type. In order to highlight their work, they used the plasticine models with grid markings engraved on it to justify this transition of mechanism through interface indentations on split blocks. The experimental results of Atkins and Tabor were utilized by Johnson [6] which led a proposition of the expanding cavity model (ECM) which has its close links to the Hill's cavity model. It describes the mean pressure for elastic-plastic solids as:

$$\frac{p}{Y} = \frac{1}{\sqrt{3}}\left[1 + ln\left(\frac{4}{3\pi}\,\frac{E}{Y}\,tan\beta\right)\right]$$ for wedge indentation

$$\frac{p}{Y} = \frac{2}{3}\left[1 + ln\left(\frac{1}{3}\,\frac{E}{Y}\,tan\beta\right)\right]$$ for conical indentation

Here β is the angle between indenter face and the sample surface

The ECM model by Johnson is a widely acclaimed model to define the deformation associated due to indentation.

Bhattacharya and Nix [18] incorporated finite element modelling and analysis to examine deformation traits related with conical indentation. This led to a revelation about the plastic strain contours, which are not of hemispherical nature. Their studies also suggested that the bulk and shear modulus also play a significant role in determining the shape and size of the deformation zone. Giannokopolus et al. [19] performed numerical simulations of Vickers indentations using FEA. They concluded that plastic strain contours depend on the strain hardening exponent 'n' and the maximum plastic strain corresponds to $\varepsilon_{p\,max}$ in close contact of to the indenter and surface in ~0.3.

Chaudhri [7]used the sub-surface indentations technique using micro Vickers indentations on annealed copper specimen. The detailed study led to develop an understanding about plastic strain distribution under spherical and Vickers indentation.

Srikant et al. [20] studied the influence of yield strength (Y) and strain hardening exponent (n) on plastic strain distribution for an Al alloy age hardened at different extents. The study was carried out for Vickers indent. The outcome of their work led to an observation that for similar values of n and higher values of Y the deformation zone is smaller while for higher values of n and same values of Y leads to a shallower deformation field. But the key finding of this work lies in the fact that plastic strain fields beneath the indenter are of elliptical orientation.

Prasad et. al. [8] utilized Chaudhry's sub-surface method in order to assess the plastic deformation beneath the conical indenter of varying apical angles (55°,65°,75°). The experimental and computational study has led to a confirmation that the shape of the deformation zone is undeniably elliptical in shape not hemispherical for annealed copper. The ellipticity of the boundary appears to be dependent on strain hardening ability of the material. As low strain hardening material exhibit high ellipticity and vice versa.

From the early 2000s various indentation studies have been done on a new class of materials i.e. the bulk metallic glasses (BMGs) to assess the details and intricacies associated to indentation. Ramamurty et.al. [21] conducted the bonded interface experiments under a Vickers indenter on Pd-Ni based BMG. The examination of this work led to a critical assessment of deformation morphology for both bulk and interface indentations. Consequently, the plastic zone sizes for both bulk and interface specimen were found to be of square root of the indentation load. Shear banded deformation regimes were observed and despite being inhomogeneous, the deformation regimes obey the idea of expanding cavity model (ECM) and hence the plastic zone is hemispherical in shape.

Zhang et. al. [11] carried out the Vickers indentation experiments on Zr-Hf based bulk metallic glasses using the bonded interface samples, they observed deformation zone's shape and size .They also proposed that Tabor's relationship and ECM of Johnson does not hold in agreement with the results obtained from Zr-Hf based BMG.

Subhash and Zhang [12] performed static and dynamic indentation on Zr-Hf based BMG they also used the bonded interface technique. Consequently, the observations of their study yields to the facts which suggest that a decrease in hardness is observed at higher strain rates in dynamic indentation contrast to static indentation. The shear bands in static indentation were accommodated as closely spaced semicircular bands, while in dynamic indentations two sets of widely spaced semicircular shear bands of different curvature were observed.

Prasad et.al. [22] studied the effect of temperature on plastic zone size and shear band density in a Zr based bulk metallic glass using a bonded interface experiment approach coupled with assessment of sub surface deformation under a Vickers indentation. The study resulted to a certain observation that the shear bands are of semicircular shape and propagate in radial direction, the inter-band spacing at all the temperatures was found to be increasing with increasing distance from the tip of the indenter.

A brief discussion is done so far about various studies and trends related the indentation experiments, which included the studies on different materials and methods like bonded interface and sub-surface indentation, which has led to the motivation for our current study on bonded interface based experiments on oxygen free high conductivity (OFHC) copper.

3.MATERIALS & EXPERIMENTAL METHODS

3.1 Materials

The material used in the experiment is oxygen free high conductivity (OFHC) of 99.99% purity in which 0.01% is oxygen. It was obtained in cast condition in the form of a rod with diameter as 3.5cm and length of 10cm, it is further annealed at 600ºC for 6 hours in a tubular furnace. From this rod after annealing two pieces of 1x1x1$cm^3$are cut. These two split pieces are to be used as a bonded interface specimen. Also, a constrained specimen of dimensions 2x1x1 cm^3 is cut with the help of wire EDM. Similarly, another set of specimens is prepared from a plate of OFHC copper of dimensions 15x15x0.634 cm^3. A strip of 15x3 cm^2 is cut and then it is further subjected to annealing operation in the tubular furnace at 600ºC for 6 hours. This is followed by cutting the strip into two equal halves, so that cold working can done for both the samples at different reduction of 33% and 45% respectively.

3.2 Sample preparation: Machining and Polishing

The cold rolling is done at a load of 11.5kN in a rolling mill, for 33% reduction in thickness single pass is done resulting in change of thickness to 0.41cm similarly for 45% reduction in thickness same rolling load is used but the number of passes required is increased to three. The thickness so obtained is 0.34cm after 45% reduction. The schematic representation of the cold working setup is given in Fig. 3.1. From both these cold worked pieces, two pieces of 1.5x1.5cm is cut using the wire EDM machining, these samples are used as split pieces for the bonded interface specimen. Also, a constrained specimen of dimensions 3x1.5cm is cut too. In wire electric discharge machining (EDM) conductive materials like OFHC copper is machined using a series of sparks produced between a moving wire (electrode) and an accurately positioned workpiece (Fig.3.2). High frequency pulses of electric current are passed from the wire to the workpiece with a very small spark gap between the workpiece and the wire which is fed continuously on to the workpiece from the spools. Due to the electric spark erosion the localised temperature in the spark gap reaches a value 8000ºC to 12000ºC causing the localised melting. Consequently, the material is removed via melting and the leftovers are flushed away by a dielectric.

The dielectric used is de-ionised water, it also acts as a cooling medium for the wire. During this operation Molybdenum wire of 0.2mm diameter is used, which is fed automatically with the help of CNC program.

The specimens so obtained are polished with SiC paper with grit size starting from 800,1000,1500,2000,2500,3000 & 5000 for a duration of 5 minutes each followed by diamond polishing for same duration with 6µm ,3µm & 1µm respectively to get a mirror finish on a Bueller Metaserv 250 polishing machine. The polishing is done at a speed of 150 to 220 rpm for the Sic paper and diamond polishing is done at 50 rpm on a velvet cloth using a lapping paste or lapping oil. The polishing is done on top and adjacent surfaces for split pieces of the bonded specimen and top and bottom surfaces of constrained specimen respectively. The top and adjacent surfaces are polished because the top surface is subjected to indentation at the junction and adjacent surfaces are joined face to face with Fevi-Kwik (Cyanoacrylate). Similarly, top surface of a constrained specimen is polished because it is the surface on which the indentation is made. Polished specimens are subjected to ultrasonic cleaning before the etching to remove any impurities present due to lapping oil or diamond paste. The ultrasonic cleaning is done with the help of Acetone which is followed by blow drying with help of blower.

3.3 Microstructural characterization

To get the microstructure, etching is done with a solution of Hydrogen Peroxide ($H_2 O_2$) 5 ml, Ammonium Hydroxide (NH_4OH) 25 ml and distilled water 25 ml. For high grain contrast a larger amount of $H_2 O_2$ (more than 5 ml to 25 ml) is used and for higher grain boundaries smaller quantity of $H_2 O_2$ is used (up to 5 ml) [23]. After the etchant preparation the specimens are etched on polished surfaces using a cotton swab for 10 to 15s followed by washing in running water and blow drying respectively .The specimens after these operations were subjected to observation under a carl Zeiss inverted axiovert 135 microscope at various levels of magnification starting from 5x to 100x to get the best possible image of the microstructure. The samples are polished and etched using the same procedure as discussed above for the annealed specimen and similar approach is followed for the cold worked specimens.

3.4 Indentation Experiments

Indentation experiments are carried out using a Samarth Brinell Hardness machine (Macro Indentation) for annealed specimens. The indentation is carried out at 7.5kN of load for both constrained and bonded interface specimen with a load cycle of 30s. For the bonded interface specimen, in order to maintain the dimensional stability and structural integrity of the bond during the indentation, the split specimens after bonding are cold mounted. The cold mounting is done with help of epoxy resin powder and hardening compound. The mount is left for curing for 6 hrs. After making indents on both the specimens, the constrained specimen is cut along the centre of the indent using Wire EDM. As far as the bonded interface specimen is concerned, it is split up by using acetone. Both specimens are again subjected to polishing discussed as above since it is a preliminary preparation for further sub-surface indentation. For the coldworked specimen macro indentation is done with help of Automatic Ball Indenter machine (ABI). The load so selected was 1.6kN for both 33% and 45% cold worked samples with a load cycle of 20s. Furthermore, same procedure is followed for these sets of specimens for wire EDM machining and cold mounting as discussed earlier for the constrained and split specimens.

3.5 Sub-surface indentations

Sub-surface indentations (Micro indentations) are carried out by using an Omnitech Vickers microhardness testing machine for both annealed and cold worked samples. Vickers indentation is performed on sectioned surfaces of constrained specimens in both annealed and cold worked samples and the same is carried out for the split specimens of the bonded interface specimens. The overall load selected for indentation is 2N with a load cycle of 20s per indentation. The indentations are done in following manner; from the periphery of the macro indent a point is selected which has a tangent parallel to the free surface of the material. From this point at 100µm beneath first indent is made which is along the loading direction. Another indent is made just beneath it at distance of 400µm and subsequently a total of 15 indents are made in a single column. Following the same steps, after the completion of column, the peripheral point just above the first indent is reached and from there the indenter is moved 300µm in positive X direction at the free surface. Again, from this point at 100µm beneath first indent of second column is made which is followed by 14 indents made in the direction of loading as discussed above.

A total of 150 indents are made in the form of a grid comprising of 15 rows and 10 columns (Fig.3.3). This is done for the annealed specimens of both constrained and bond interface type. A similar kind of micro indentation procedure is followed for cold worked samples as discussed above with same load of 2N and load cycle of 20s per indentation. The only difference is a total of 40 indents are made in the form of a grid comprising of 8 rows and 5 columns (Fig.3.4).

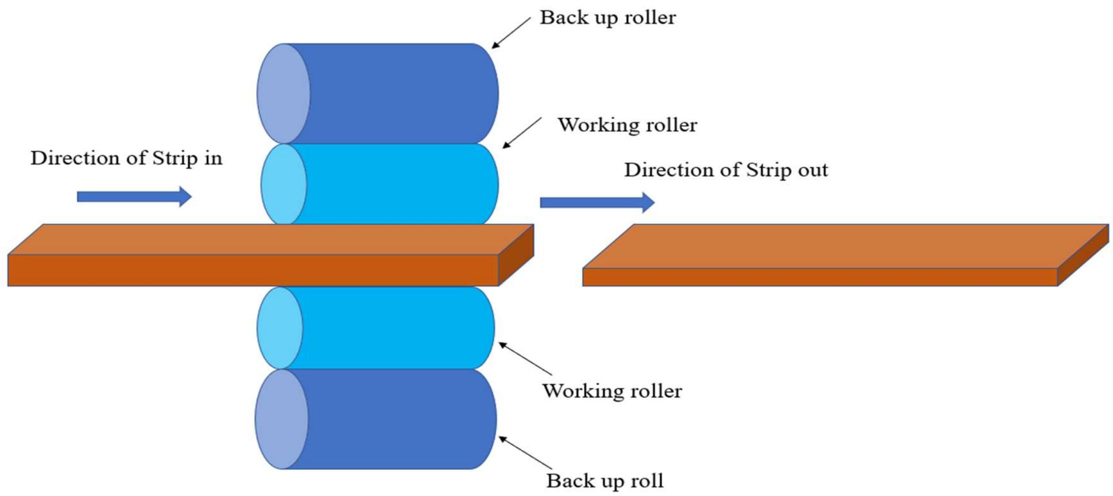

Fig.3.1 Schematic of Cold rolling setup

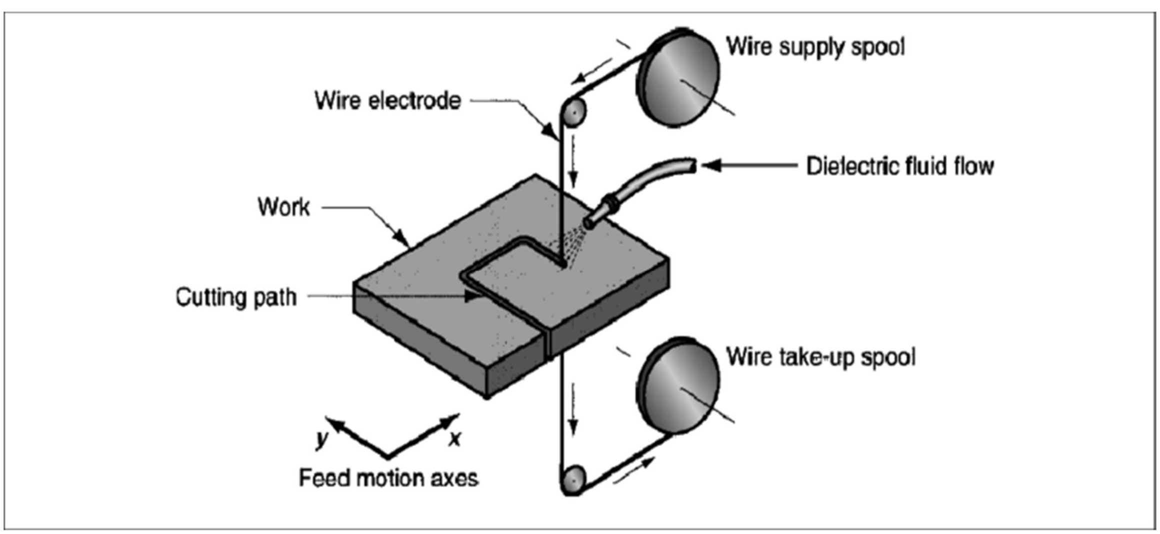

Fig.3. 2 Wire EDM Schematic Setup

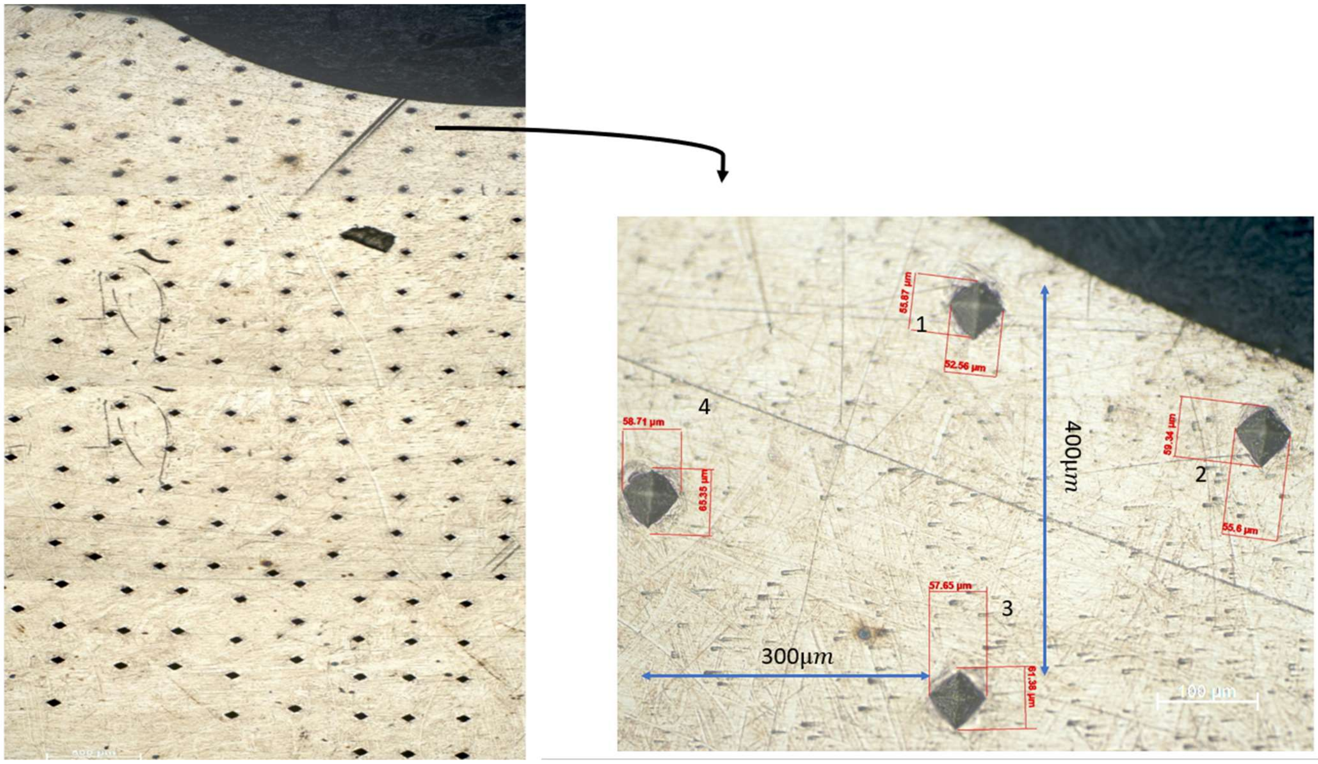

Fig.3.3 Sub-surface indentation of annealed specimens

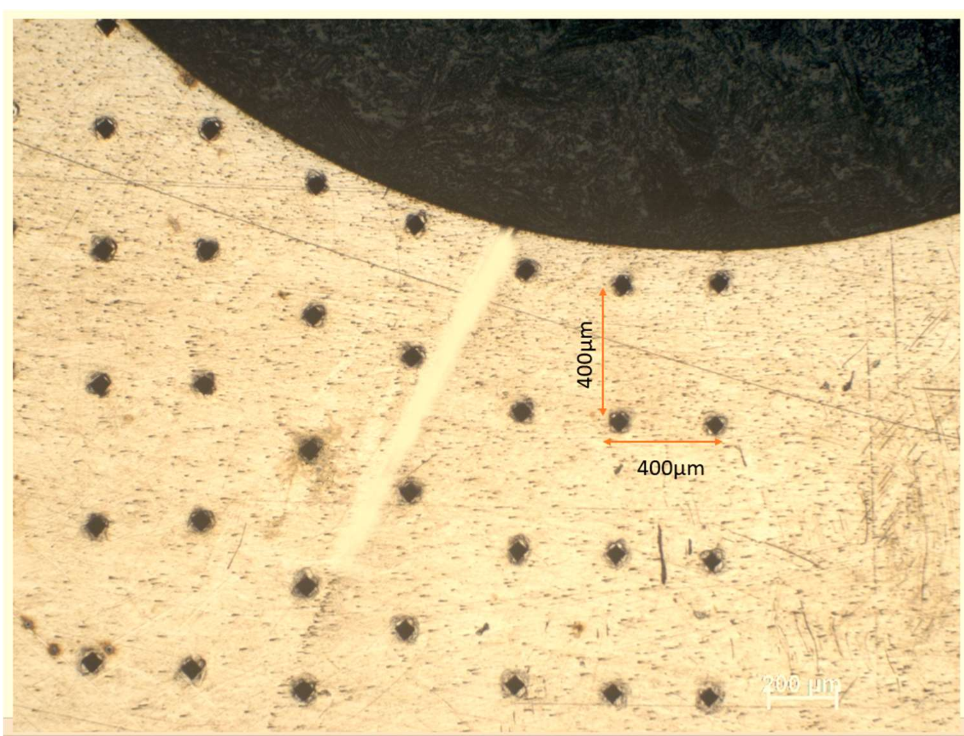

Fig.3.4 Sub-surface indentation of cold worked specimens

4.MODELLING METHODOLOGY

The finite element analysis of the constrained and split configuration is done by using ABAQUS/CAE 6.14-5 2014 version software. For both the configurations 3D modelling is done. In constrained specimen in order to have 3D OFHC copper block, a 3D deformable revolution model is used. Initially, a rectangular lamina of dimensions 50x25mm is drawn and further it is rotated by 90° to get a 3D quarter of a cylinder with height of 50mm and radius of 25mm (Fig.4.1a). The height or depth is 10 times the diameter of the indenter which is of 5mm and hence 50mm is chosen for the modelling. At the topmost surface of the OFHC copper block, a partition is created in the form of a square which is extruded along the depth of the specimen. Further moving down along the corner point or the vertex of the cylinder beneath the indenter, another partition is created, thereby a rectangular prism is obtained which is bifurcated into two regions. The region beneath the indenter is a cube of 10.6mm side which is extended to the same distance beneath the top surface of the OFHC copper model as given in figure 4.1. The same approach is incorporated for the split specimen model the only difference being a separated by a section of glue layer (Fig.4.1b). The glue layer is assigned in a section on XY-plane with thickness of 30µm and it extends along the entire depth of the copper model. The indenter of 5mm diameter as mentioned above is used with 3D rigid shell type model for both specimen configuration. The indenter's Youngs modulus E is taken as 600GPa and poisons ratio ν as 0.22. For OFHC copper E is taken as 120GPa and ν as 0.3. For OFHC copper the plastic properties are obtained from tensile testing. For super glue E is taken 1.5GPa and ν as 0.3.

During the analysis, for both constrained and split models contact type interaction is defined coefficient friction being 0.4 between the contact surfaces of indenter and OFHC copper. The boundary conditions are chosen as the base in XZ-plane being fixed for both the configurations. In XY-plane, displacement along Z direction and the rotations along X, Y and Z direction is arrested respectively. Similarly, in YZ-plane displacement along X direction and the rotations along the X, Y and Z direction is arrested respectively. These boundary conditions are utilised for both the configurations i.e. constrained and split specimen (Fig.4.2). The regions of boundary conditions where the displacements and rotations are arrested represents the regions where the metal is present. Moreover, this metal is providing these resistances in various planes in the form of boundary conditions. Only a quarter is modelled in order to reduce the computational time.

The meshing is done in such a manner that elements are fine in the cube partition in both constrained and split specimens. In split specimen one the sides include the glue layer also. A total of 74450 elements are utilised for constrained specimen (Fig.4.3) and 69300 elements are used for split specimen (Fig.4.4). Both the scenarios used C3D8H elements, the designation can be further classified as C for continuum type 3D element having 8-node hybrid formulation. Indenter is modelled with 166 elements for both the scenarios with R3D4 element type which is 4 node 3D bilinear rigid quadrilateral element. The indenter is given a displacement-controlled movement in vertically downward direction in the direction of loading in both cases. The displacement of 1.45mm is assigned as a boundary condition keeping all other rotation and translation fixed. The value 1.45mm is chosen because the depth of the experimental indentation corresponds to this value. Von-Mises criteria of deformation is used in both the simulations.

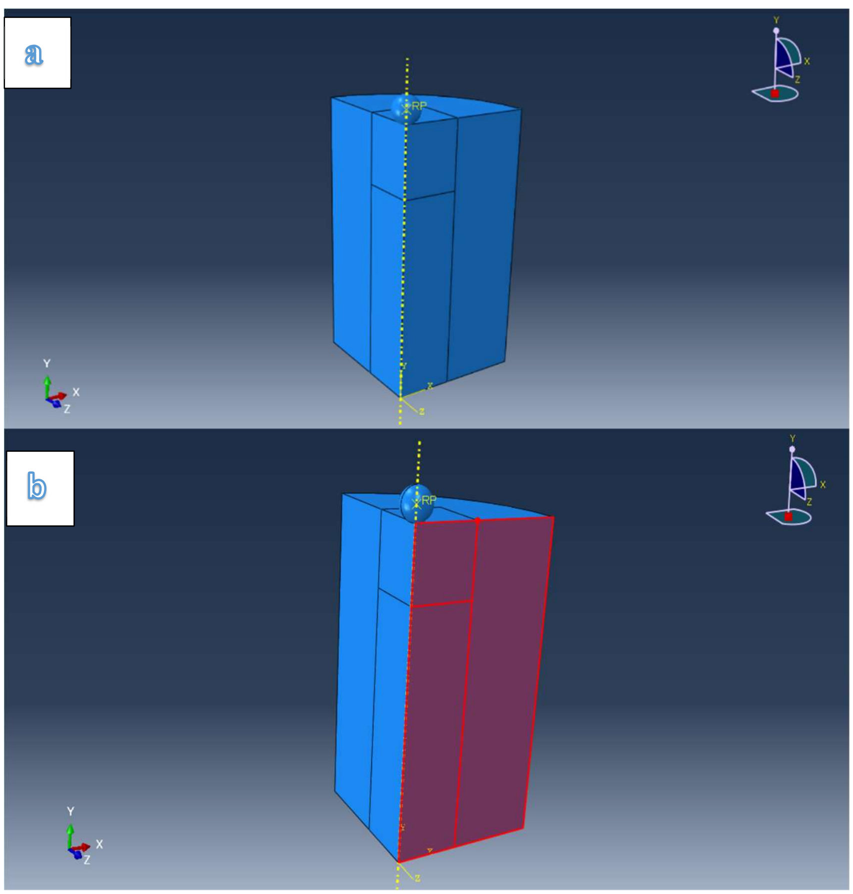

Fig.4.1 a). Constrained specimen assembly b). Split specimen assembly with glue layer

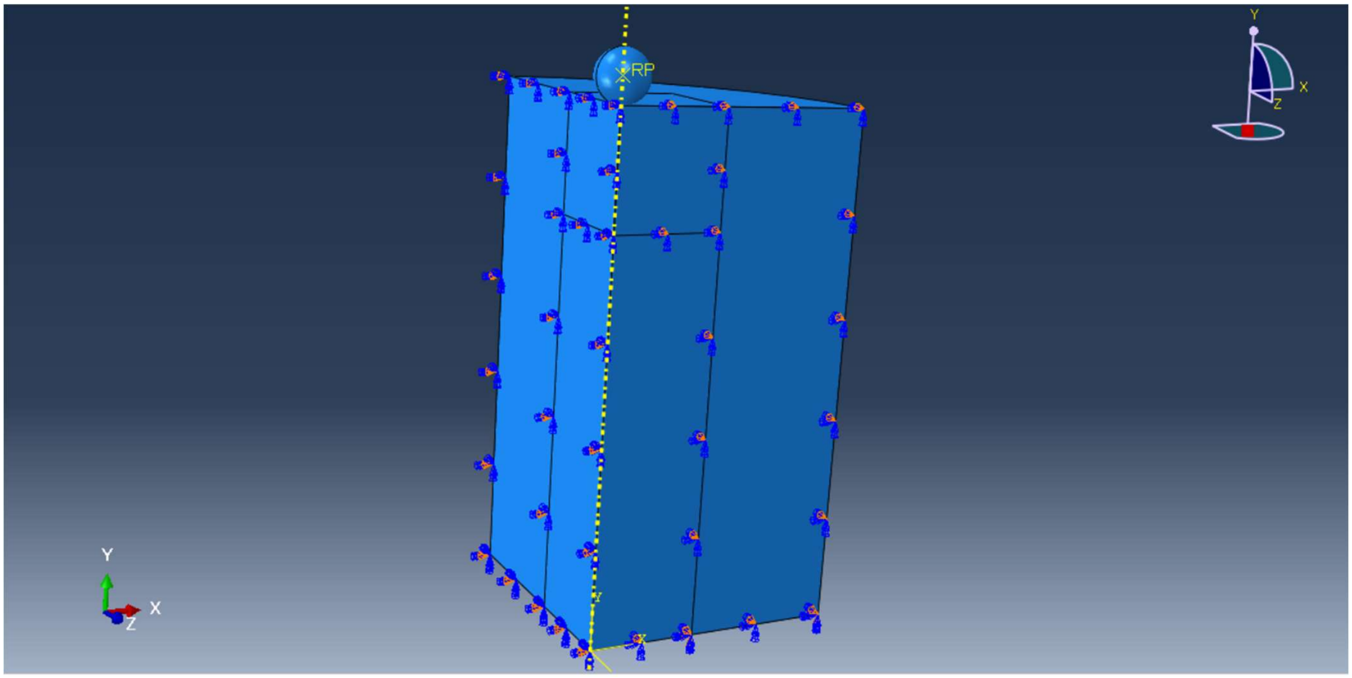

Fig.4.2 Boundary conditions for constrained and split specimens

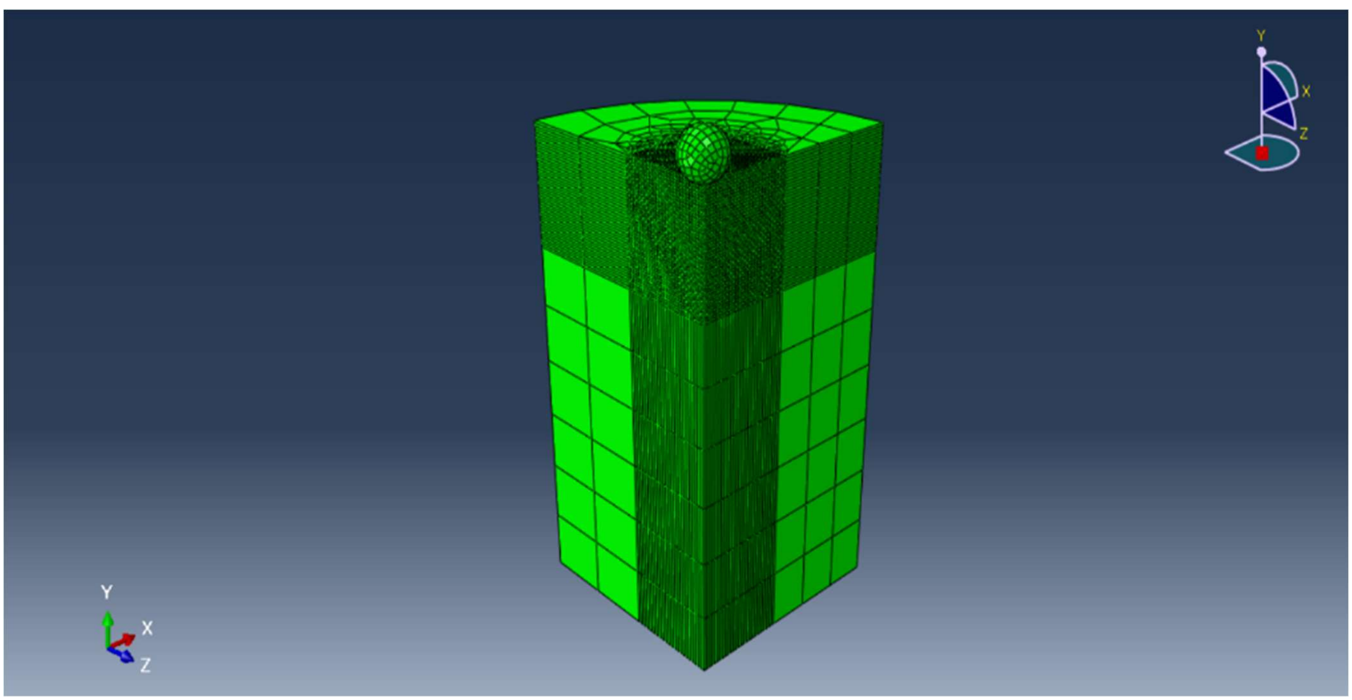

Fig.4.3 Meshing of constrained specimen assembly

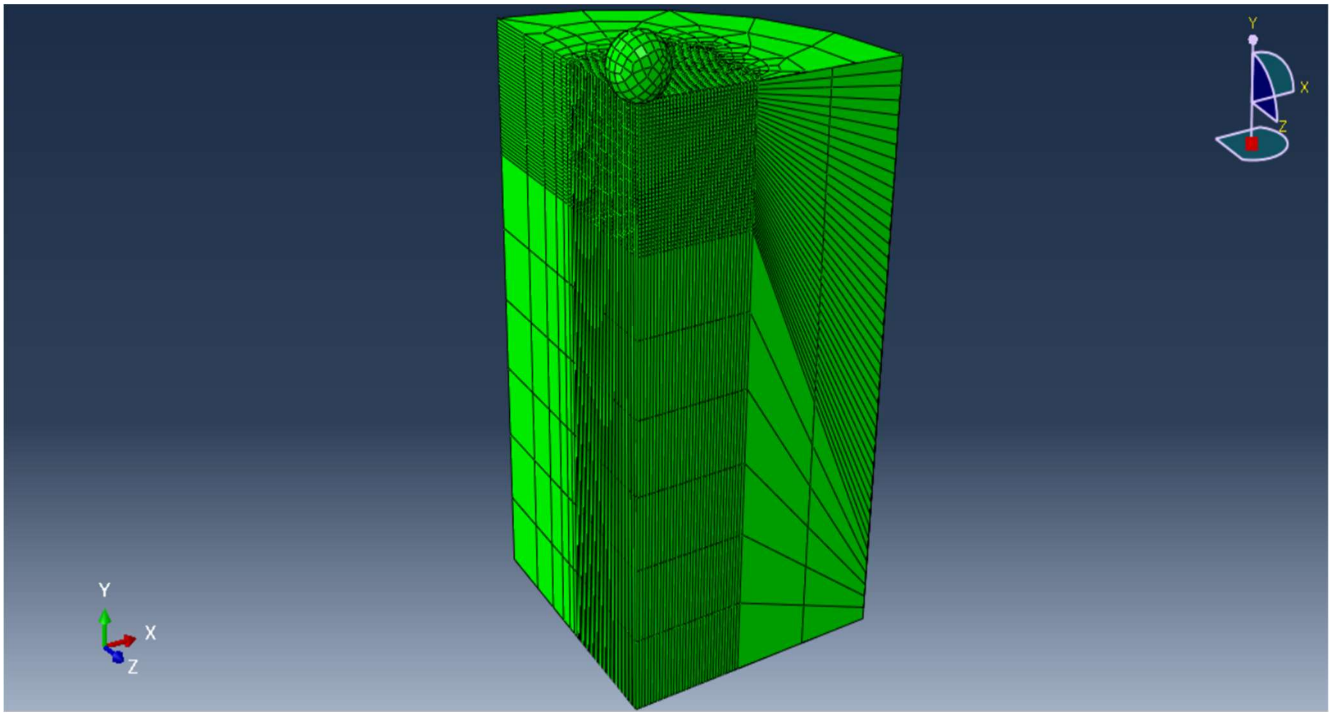

Fig.4.4 Meshing of split specimen assembly with glue layer

5. RESULTS

5.1 Microstructures

The microstructural analysis is done after carrying out all the necessary metallographic operations viz. from polishing to chemical etching. Beneath the indenter it is observed that there is a substantial change in the microstructure, and it exhibits unique characteristics. Approximately 100µm beneath the periphery of the macro indent and along the indentation axis a region of severely deformed grains is observed (Fig.5.1). The distortion in grains is clearly seen in the form of clusters, which are formed due to indentation. Due to the indentation localized defects dislocations, twins stacking faults are formed due to which a region of severe deformation is formed. In this region of severe deformation, the morphology of individual grains is unresolvable.

Further away from the indenter, outside the highly strained region as discussed above at a depth of around 6.5mm a change in the morphology of the grains is observed (Fig.5.2), These grains corresponds to the bulk metal which is only in annealed condition and the effect of deformation due to indentation is diminished in this region. This can account for the fact that metal in this zone is far away from the vicinity of the indentation and hence the extent of plastic deformation decreases significantly due to less strain hardening in comparison the region beneath indentation. Also flakes of copper is observed along with twins formed due to annealing. The reason for this could be that during annealing recovery, recrystallisation and grain growth takes place. In the recovery phase the metal undergoes softening due to which the residual stress present in the metal gets released, at this point the grain is not affected. Recovery is followed by recrystallisation in which new strain free grains are formed due to nucleation, these newly formed grains replace the grains completely to a new set of grains which are free from any strains. After recrystallisation during annealing grain growth takes place consequently the grain size increases.

The cold worked samples which were subjected to 33% and 45% reduction were also studied microstructurally. Both the specimens were subjected to same annealing conditions as discussed in previous section. During the cold working the specimens go through multiple passes of rolling. This results in squeezing of the samples causing a change in the grain size.

For a 33% cold worked sample the grain size is found to be 53±30µm (Fig.5.3) while for a 45% cold worked specimen the reduction is 37±20µm (Fig.5.4). This phenomenon of variation in grain sizes can account for the fact that cold working increases the yield strength and hardness of the metal. As a result of this defects are introduced into the crystal structure of the metal. Due to the compression between the rollers the dislocations get arrested thereby preventing active slip leading to hardening of metal.

A SEM image of 45% cold worked specimen is shown in figure.5.5 for a bonded interface configuration. As it is clearly seen from the image that deformation of copper is occurring via formation of slip bands occurring due to severe localized deformation caused by indentation. The localization is caused by accumulation of dislocations in a region, subsequently the slip lines come close to one another causing the dislocation line to bow around leading to formations of striations or slip bands [orowan]. The protrusion of metal is seen because due to loading the metal beneath the indenter flows. Since the bonded interface is weak at the glue section, the flow of metal facilitates itself along the direction normal to the split surface. An elliptical cavity is formed as the interface offers a path of least resistance.

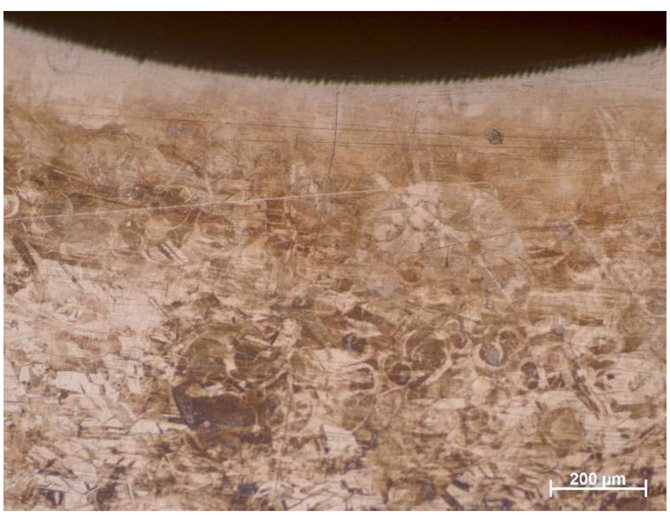

Fig.5.1 OFHC copper beneath the indent

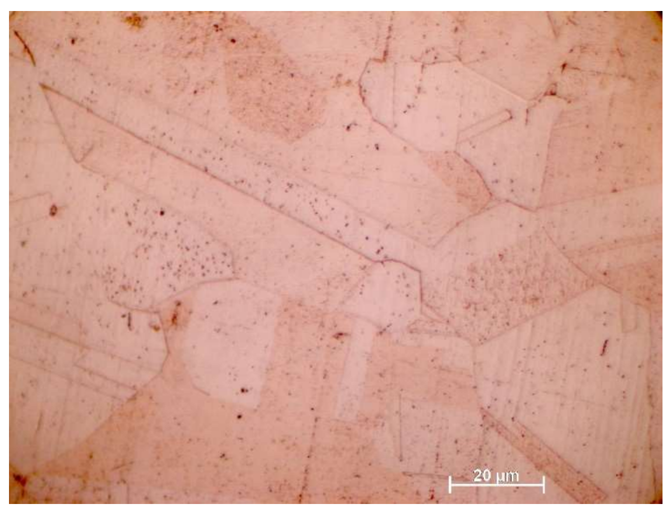

Fig.5.2 OFHC copper far from the indent

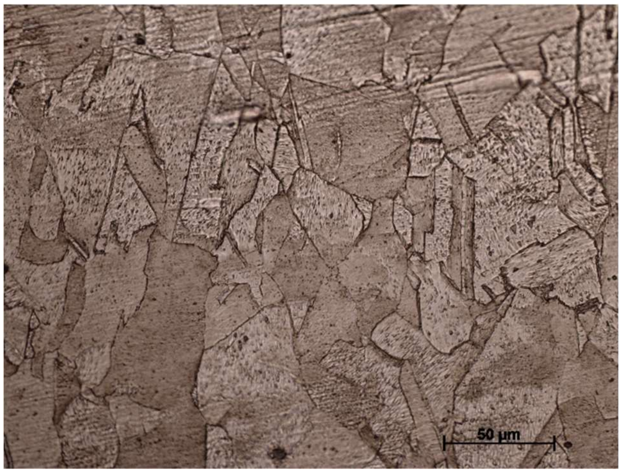

Fig.5.3 33% cold worked OFHC sample

Fig.5.4 45% cold worked OFHC sample

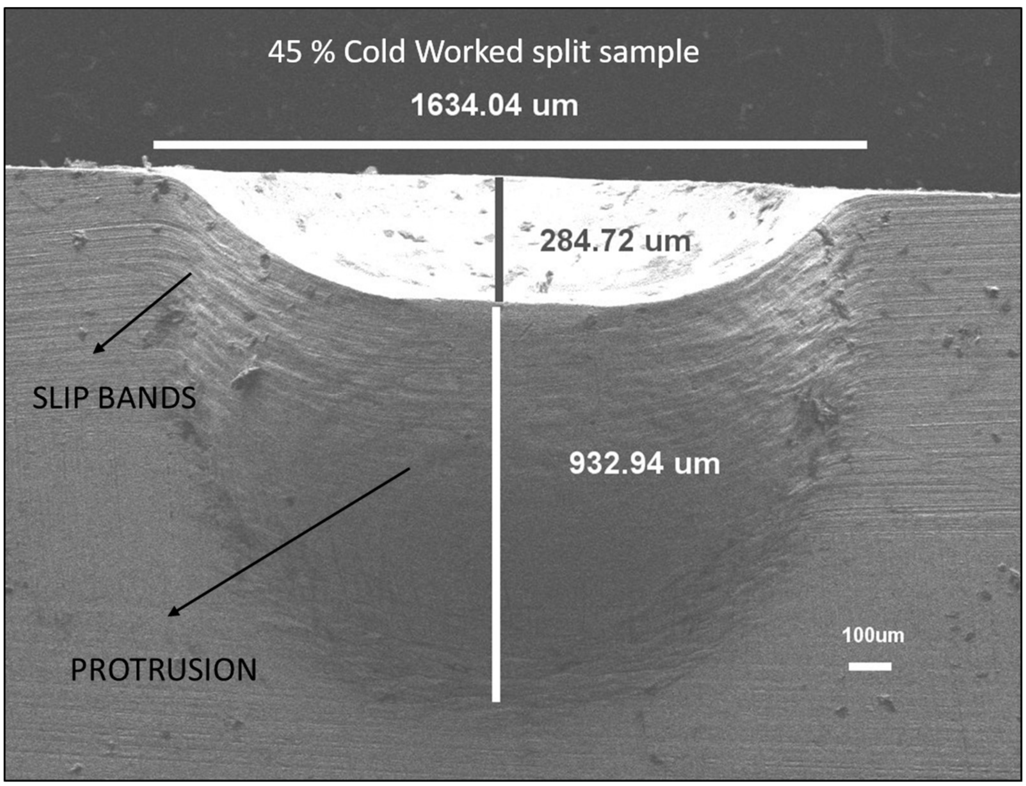

Fig.5.5 SEM image of 45% cold worked specimen

5.2 Sub-surface indentation mapping

The sub-surface indentation mapping of annealed and cold worked samples is obtained for both constrained and bonded interface configuration. For the annealed specimen the hardness values obtained from micro Vickers indentation are converted into equivalent plastic strain by using the relation H=132$\varepsilon^{0.2}$ [8]

5.2 .1 HARDNESS MAPS (CONSTRAINED and SPLIT SPECIMEN)

5.2.1.1 Annealed Specimen

For both the specimen configuration i.e. constrained and split or bonded interface a macro indentation is made with 7.5kN load. Micro indentation is done by using 2N load applied by a diamond indenter of Vickers type. The distance between two indenters is 400μm in vertically downward direction and 300μm is the distance between two adjacent indents (Fig.3.3). The hardness mapping of annealed constrained specimen indicates that in vertically downward direction along the indentation axis at 5.8 mm from the indenter periphery the hardness obtained is equal to the bulk metal hardness. This signifies the extent of hardening that has occurred due to indentation. This trend continues for first three columns, but on moving further in +X direction of rest of the columns the extent of hardening becomes shallower as more frequently the value of bulk metal hardness is obtained at depth of 4.8mm. Similarly, moving in horizontal direction the hardness values show a higher magnitude for first six values of corresponding six columns of indents. The later four values of rest of the columns show a decremental trend. The second value of hardness for every column is higher than the first value (Fig.5.6). Using the power law of hardening as mentioned above, corresponding strain values are obtained. The values of strain follow the same trend as that of the hardness values as discussed above. For a split specimen configuration (Fig.5.7). the values and trend for hardness is not varying too much in comparison constrained specimen and a similar trend is observed in strain values.

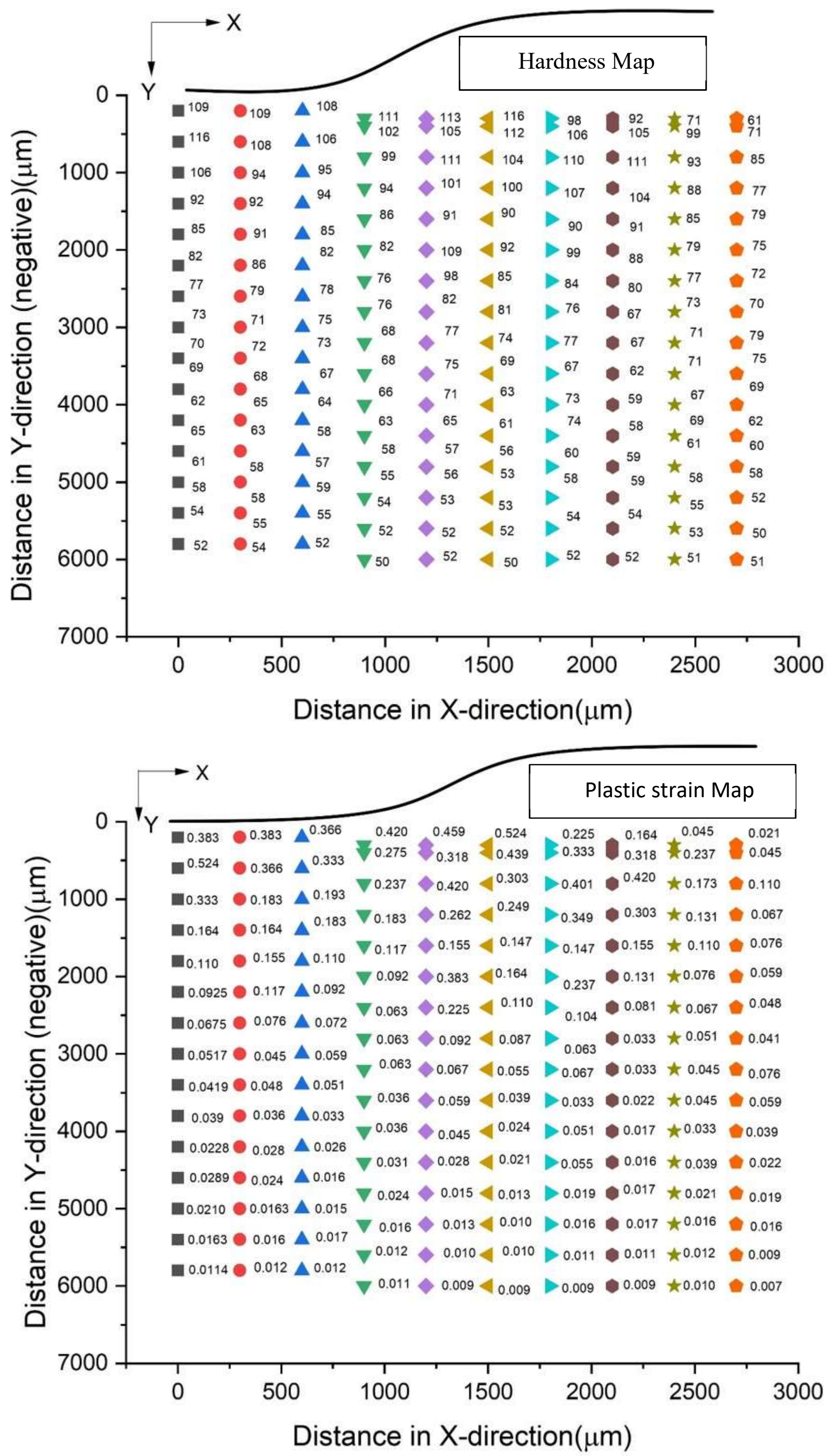

Fig.5.6 Sub-surface indentation map with hardness and plastic strain values: Constrained specimen

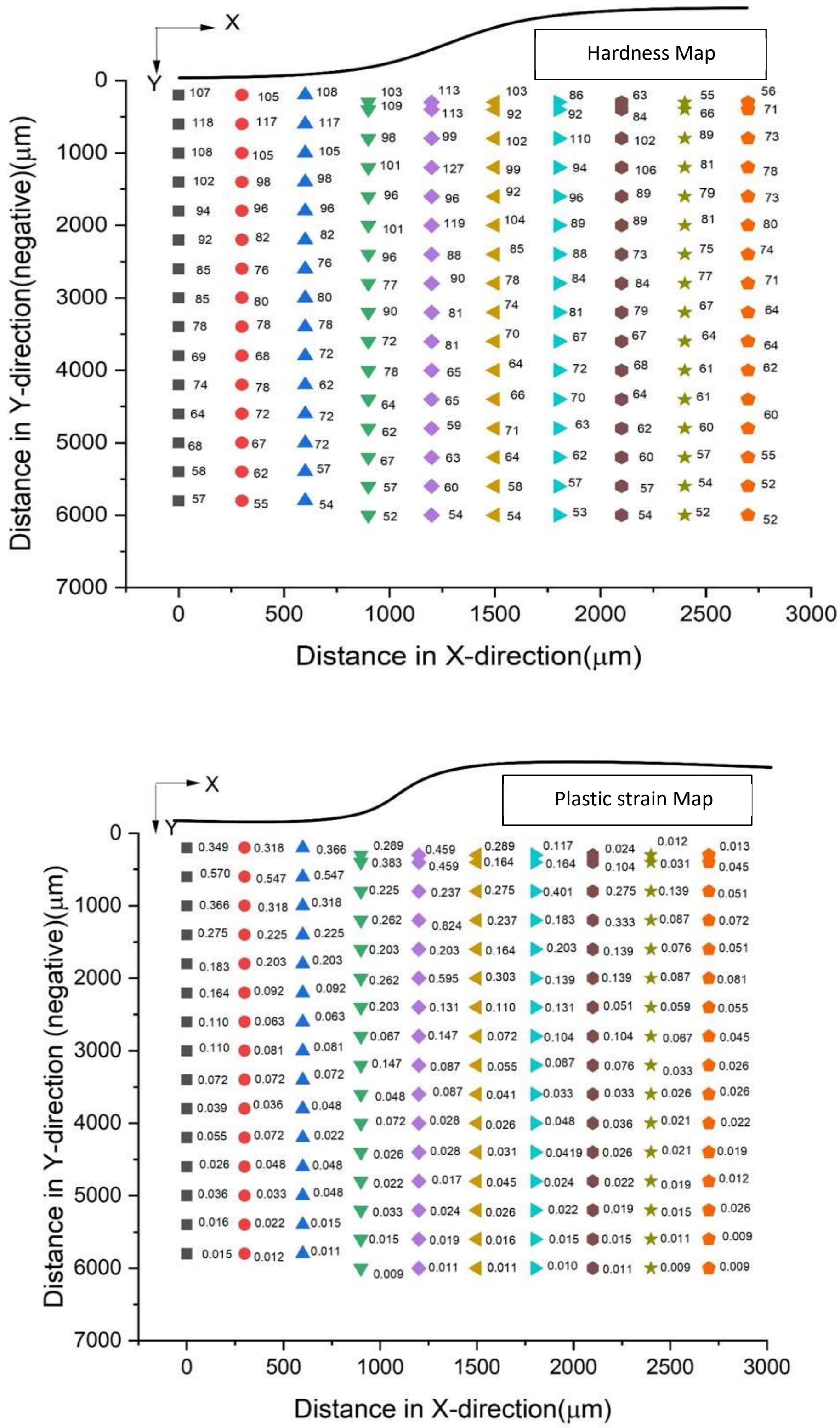

Fig.5.7. Sub-surface indentation map with hardness and plastic strain values: Split specimen

5.2.1.2 Cold worked Specimen

The hardness maps of both cold worked samples (33% and 45%) for constrained and split configuration is obtained by using micro Vickers indentation with a load of 2N. The macro indentation is done at load of 1.6kN. The distance between two vertical and horizontally adjacent is indenter is taken to be 400μm each (Fig.3.4).

For both the cold worked specimens it is observed that hardness values do not show a significant variation as it is observed for annealed specimens. This is seen for both split and constrained configuration (Fig.5.8 and Fig.5.9). The plausible reason for this can be; OFHC copper may have got completely hardened during 33% cold working therefore due to hardening the variation in hardness values is insignificant. Similar conclusion can be drawn for 45% cold worked specimen. Hence the metal is behaving like an elastic-perfectly plastic material due to cold working in both the samples.

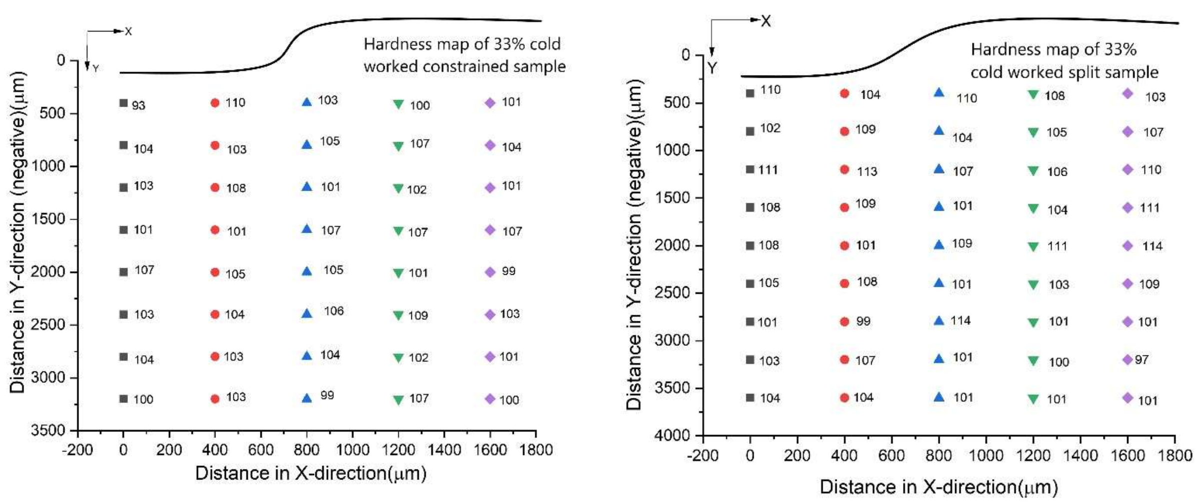

Fig.5.8. Hardness maps of 33% cold worked samples

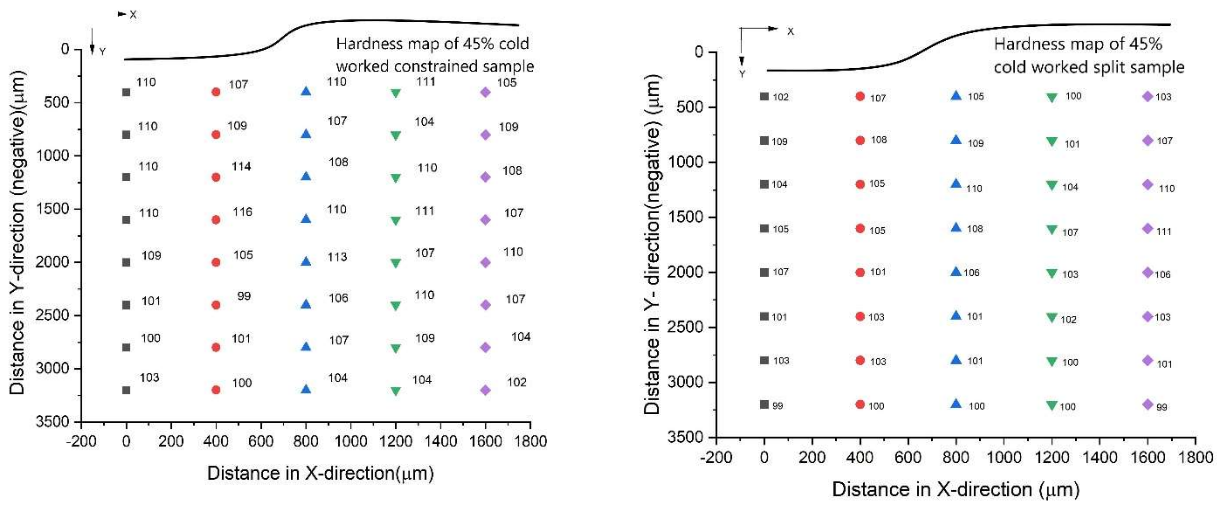

Fig.5. 9 Hardness maps of 45% cold worked samples

5.2.2 Strain contours (Annealed constrained and split specimens)

The plastic strain distribution around the sectioned indented surface is visually represented by iso-strain contours as shown in figure 5.10 [8], [20]. The contour lines drawn here are merely schematic representation, a guide to the eye. Here all the distances are normalized, obtained by dividing the distances from the indenter center by the diameter of the indenter (d). It is evident from the figure that the spread of the plastic strain around the indentation axis is in vertically downward direction. The spread is also observed along the radial and horizontal direction. The observable trend of strain values shows a decaying trend for both the specimen configuration i.e. constrained and split.

5.3 Plastic strain decay

The nature of strain decay beneath the indenter is determined for both constrained and split samples. In figure 5.11 plastic strain values are plotted against the normalized distance for both the configurations for all the rows. For a constrained system the strain values have a relatively less scatter in comparison to the split system. The strain values of high magnitude are obtained nearer to indentation periphery. The decay pattern for a constrained specimen in the rows away from the indentation and the rows near to the indentation axis corresponds to almost similar strain values.

On the contrary, for a split specimen configuration the strain decay is systematic for first four rows, after that the rows five to eight experience low strain values with least strain values in the last two rows.

To have more clarity and understanding of the decay behavior, only first four rows of indentation is being plotted in figure 5.12 for constrained and split specimen respectively. It can be observed that for a constrained specimen all for rows beneath the indent follow a smooth decaying curve and in the range of 0.6 to 1 of normalized distance along the depth all four rows have same strain values. For split specimen, the scatter in the strain values is on the higher side in comparison to constrained specimen. Moreover, for the 4th row of indentation, the values are highly scattered in contrast to constrained specimen. Another assessment of plastic strain vs normalized distance is done just beneath the indenter for a single row of indents for both the configurations in figure 5.13 The decay of plastic strains in this context is almost similar with only miniscule differences present.

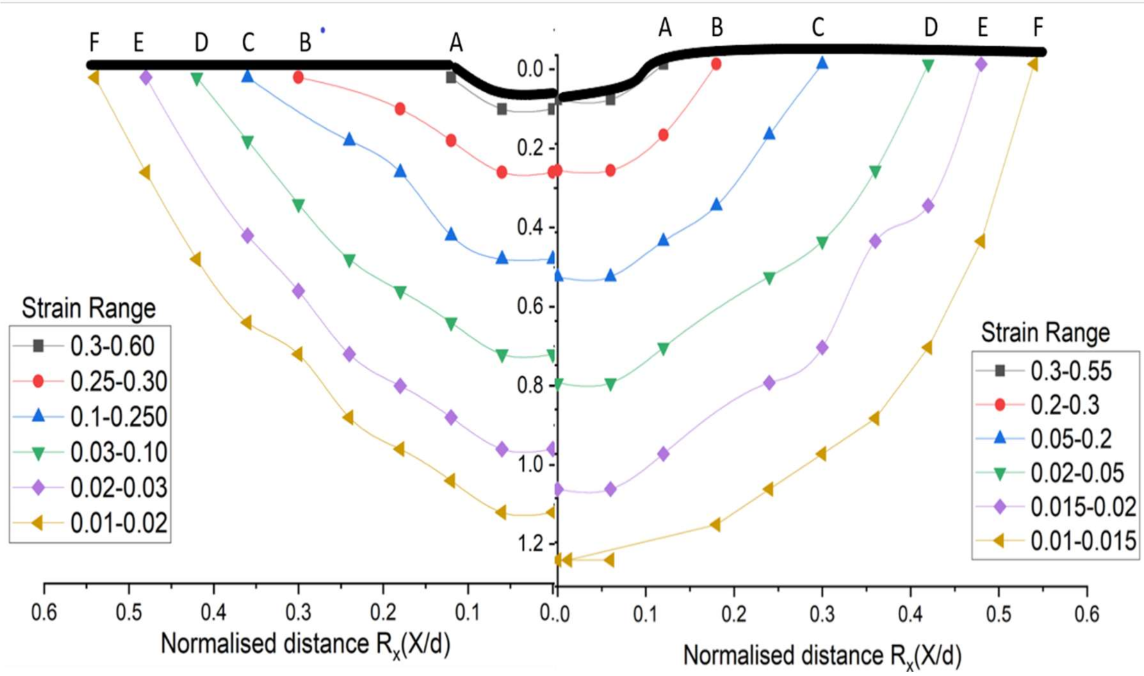

Fig.5.10. Strain Contours: Split Specimen (Left) vs Constrained Specimen (Right)

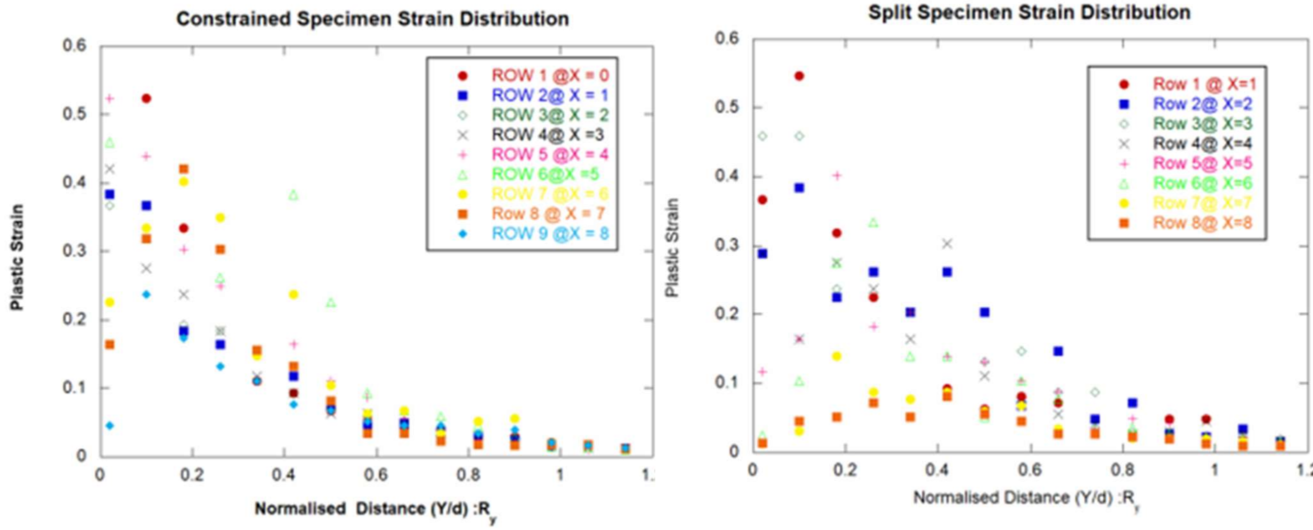

Fig.5.11. Comparison of strain distribution of constrained and split specimens

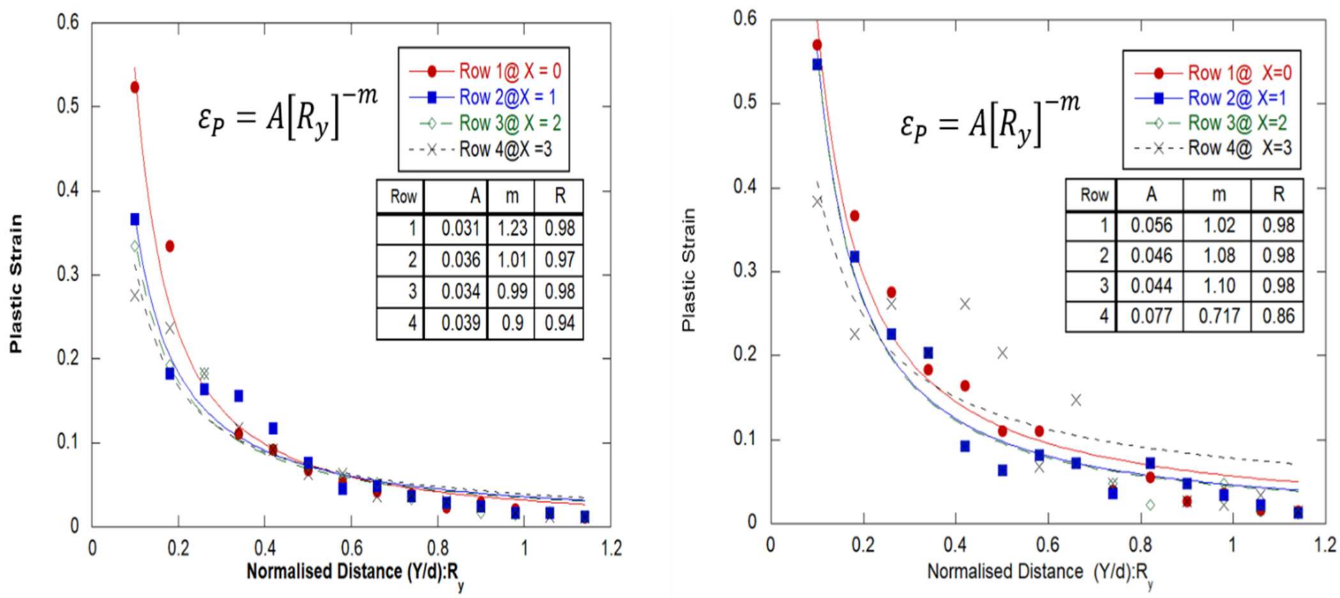

Fig.5. 12. Strain decay up to first four rows: Constrained (left) and split specimens (right)

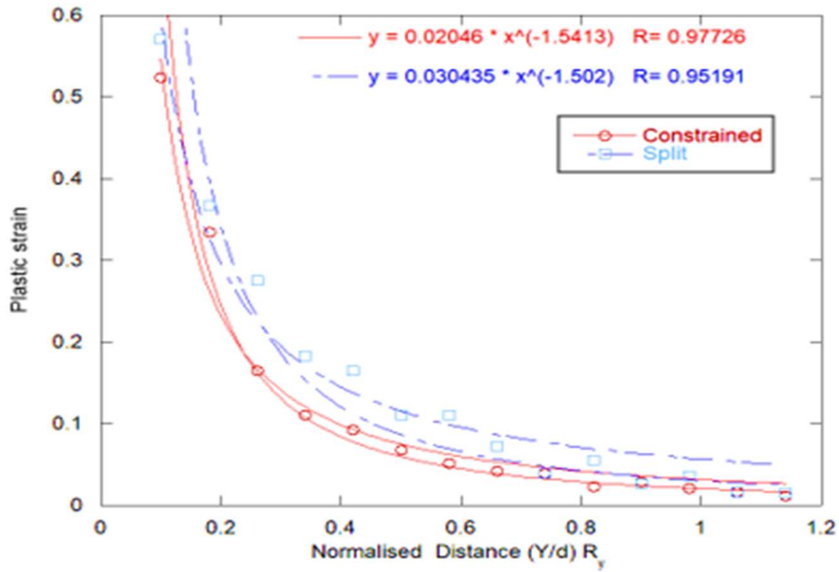

Fig.5. 13 Strain decay for constrained and split specimen along the indenter axis

5.4 Simulation results

In this section a discussion related to the simulation results is done. The figure 5.14 represents the plastic strain equivalent obtained from the simulation of a constrained specimen configuration. The range of strain developed due to indentation on OFHC copper block is ranging from a maximum value of 1.84, this strain corresponds to the surface just beneath the indenter. The minimum indentation strain is 0.01 which ultimately diminishes to 0, thus representing the extent of the plastic deformation. In figure 5.15 plastic strain equivalent corresponding to the split strain configuration is attained. The split specimen simulation shows a relatively lesser maximum strain value of 1.39 beneath the indentation in contrast to its counterpart. However, the minimum values being same 0.01 which also diminishes to 0. This variation in the maximum strain values can be associated with a weaker metal- glue interface in the split specimen.

In figure 5.16, comparative analysis of plastic contours on constrained and split specimen is done. This comparison is done for constrained and split configurations based on simulations only. It is seen that for constrained specimen the deformation depth is more in contrast to the split specimen.

Also, in split specimen system the deformation zone experiences a significant lateral spread than the constrained specimen.

In figure 5.17 a comparison is done between simulated experimental results for a constrained specimen configuration. The experimental observations clearly indicate a deeper deformation zone in contrast to the simulated observations. Also, the experimental findings show iso-strain contours in the form of strain ranges, while for simulated results contour lines of constant strain values are seen. Similarly, in figure 5.18, the split specimen configuration also shows similar trend for the depth deformation with experimental depth of deformation being larger than the simulated depth. But as far as the lateral spread of the deformation zone is concerned, the simulation shows a wider spread in comparison to experimental results for the split specimen configuration. For both the configurations, simulation results show a closed contour line orientation in comparison to experimental results.

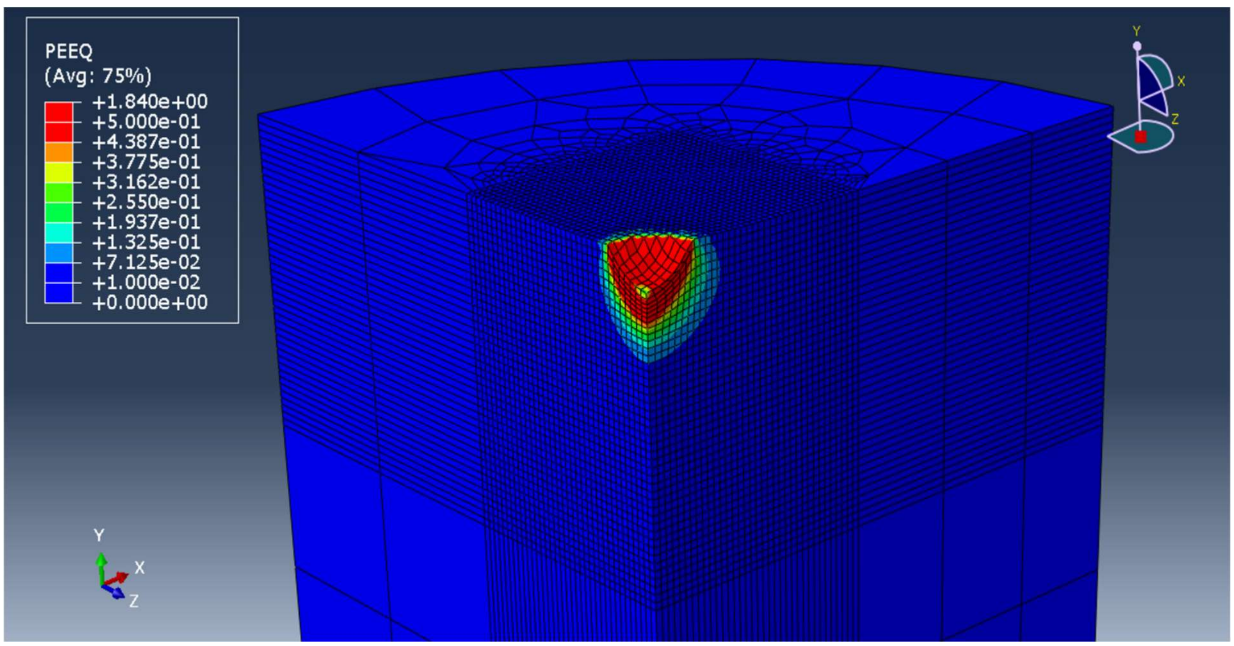

Fig.5. 14 Constrained specimen plastic strain equivalent (PEEQ)

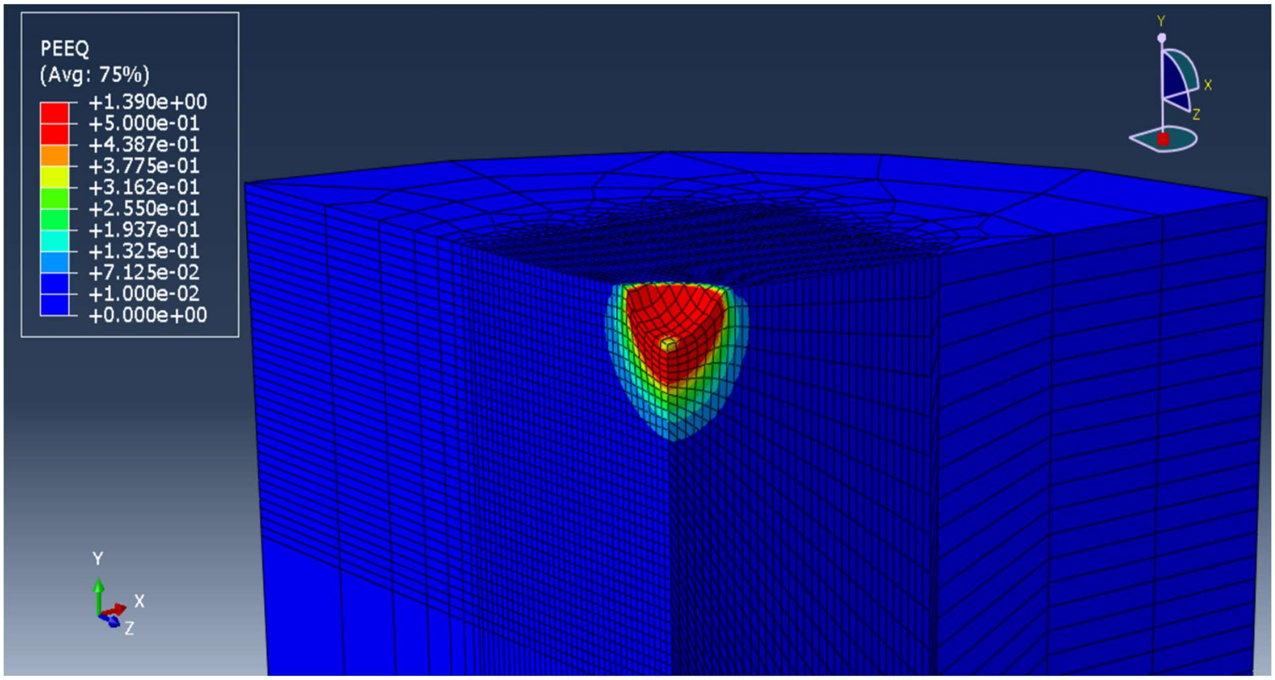

Fig.5. 15 Split specimen plastic strain equivalent (PEEQ)

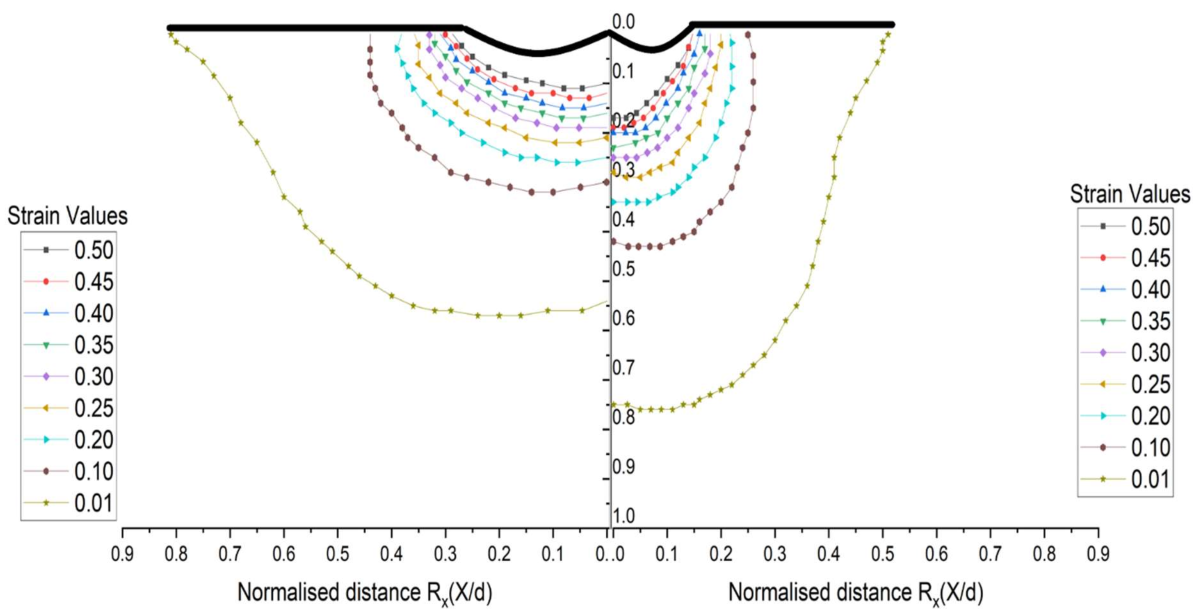

Fig.5. 16 Split specimen(left) vs Constrained specimen (right) *simulation results* of plastic strain equivalent (PEEQ) on the sub-surface

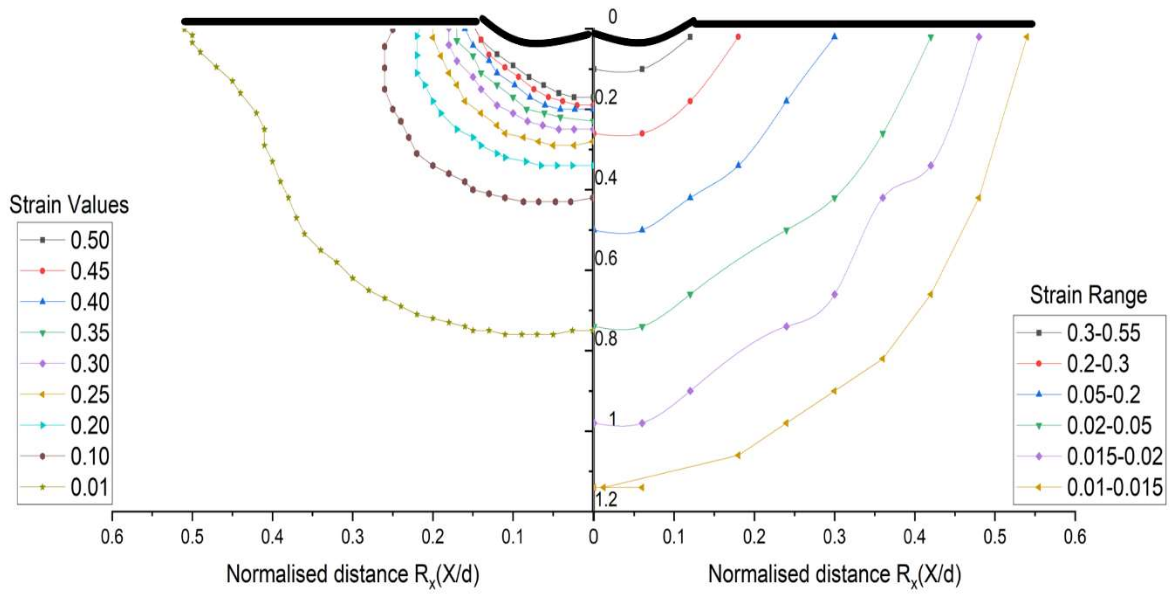

Fig.5. 17 Constrained specimen: Simulation (left) vs Experiments (right) results of plastic strain equivalent (PEEQ) on the sub-surface

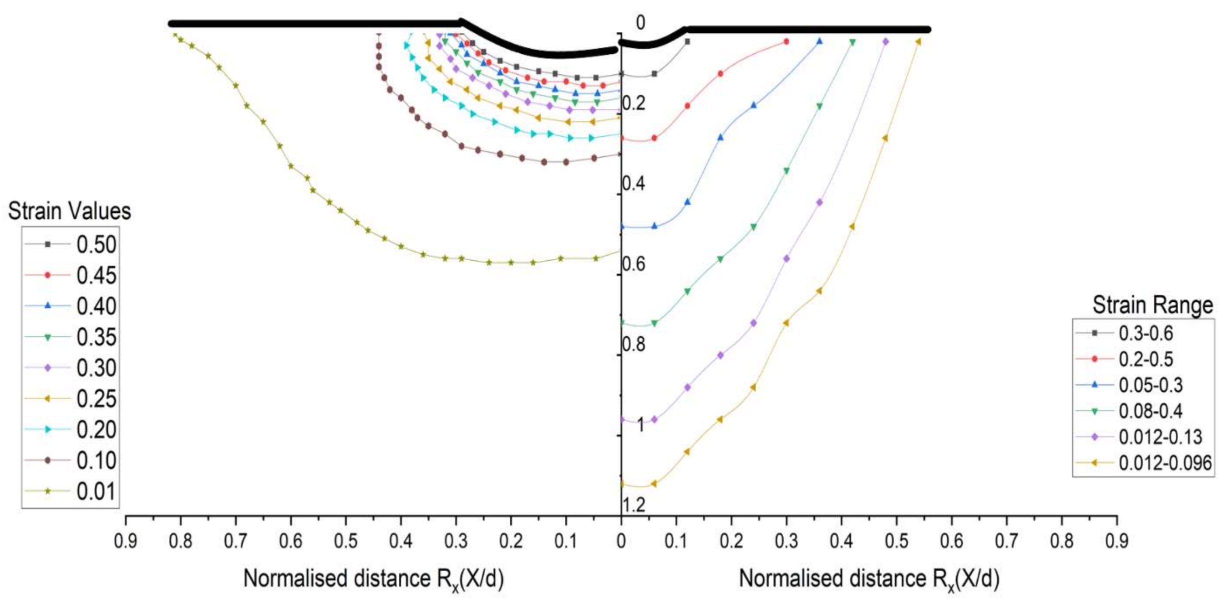

Fig.5. 18 Split specimen: Simulation (left) vs Experiments (right) results of plastic strain equivalent (PEEQ) on the sub-surface

6. DISCUSSION

6.1 Comparison between constrained and split specimen strain contours

From the hardness maps obtained in figures 5.6 and 5.7 it is observed that the first hardness values in every column is less than the second values. It can account for the fact that these values are in proximity with the free surface of the metal and it is not surrounded by metals from all sides. Due to which when indentation load is applied, along the free surface the hardening is not dominant enough and hence the lower values are seen for both the configurations. The same reason can be held accountable for the respective plastic strain values which demonstrate a similar trend like the hardness values.

A comparative study of plastic strain contour is also carried out in figure.5.10 for the experimental observations of both the configurations. From these contour plots it is seen that the range of plastic strain is almost similar, the only difference being, in constrained specimen due to homogeneity of the material along the indentation axis or the loading direction the extent of deformation or the depth of deformation is more in comparison to its counterpart of split specimen. In a split specimen the extent of deformation is on the shallower side because of the inhomogeneity or heterogeneity present along the direction of loading due to the presence of superglue. Moreover, the glue is the weak link at the interface and hence during the loading the effect load is transferred laterally onto the surface. The iso-strain contours for both set of specimen configuration clearly indicate that the shape of the plastic zone is of elliptical nature. In order to quantify this proposition a term ellipticity ζ is used. This quantification is already done by Prasad [8] and Srikant [20]. The parameter ellipticity ζ can be defined as the ratio of normalized distances along Y and X-directions. The values of ellipticity of split and constrained configuration is given in table 2 and 3. According to Prasad and Srikant, $\zeta=1$ for Johnson's expanding cavity model (ECM) and hence the state of elastic-plastic boundary is of hemispherical nature. From the table 2 and 3, the values of ζ are coming out to be greater than 1 for most plastic strain contours in both configurations suggesting that the assumption made as per ECM about hemispherical deformation zone is inaccurate.

The experimental strain contours (Fig.5.10) signify that for OFHC copper in annealed state is a low strain hardening metal and therefore deformation is extended more along the indentation axis in both the specimen configurations. Since the material beneath the indenter offers a less resistance to plastic deformation imparted by the indentation load. Consequently, the material with low values of hardening exponent *n* exhibit higher ellipticity and vice-versa.

The plastic strain decay plots in figure 5.12 suggests that the strain decays rapidly along the depth of indentation and the power laws are sufficing for this decay for the experimental results. The fit parameters are listed in the inset tables in figure 5.12. In this inset tables *A* values show the metal's resistance to deformation. The *A* values are showing a marginal change in constrained configuration while for split configuration the variation is showing a certain significant change. The *m* values in both cases corresponds to the decay exponents. Constrained specimen shows a decremental decay due to material homogeneity while for split specimen the decay is rather erratic and thus it can be accounted for the inhomogeneity associated due to metal-glue interface. The *R* values of regression constant, for a constrained specimen for all the four rows are nearing 1 which implies that the curve fitting is a nearly good fit to explain the decay behavior, whereas for split specimen values of the fourth row implicate a poorer fit and hence the scattered points are obtained.

Table 2 Ellipticity of constrained strain contours (Fig. 5.10)

Contour lines	Vertical Normalized Distance (R_y)	Horizontal Normalized Distance (R_x)	Ellipticity (ζ=R_y/ R_x)
A	0.10	0.12	0.833
B	0.26	0.18	1.44
C	0.50	0.30	1.66
D	0.74	0.42	1.76
E	0.98	0.48	2.04
F	1.14	0.54	2.11

Table 3 Ellipticity of split strain contours (Fig. 5.10)

Contour lines	Vertical Normalized Distance (R_y)	Horizontal Normalized Distance (R_x)	Ellipticity ($\zeta = R_y / R_x$)
A	0.10	0.12	0.833
B	0.26	0.30	0.866
C	0.48	0.36	1.330
D	0.72	0.42	1.714
E	0.96	0.48	2.000
F	1.12	0.54	2.074

6.2 Simulation vs Experiments

The simulation and experimental studies conducted on the constrained and split specimens points out to the fact that the shape of the deformation zone associated with spherical indentation is of elliptical nature. This is in concurrence with the findings of Prasad et.al. [8]. It is observed from figures 5.16 and 5.18 that the simulation results show a shift in the deformation zone away from the load axis predominantly into the body of the specimen laterally. It can be explained by the following proposition that when the metal-glue interface is subjected indentation load, the glue layer collapses and thus the load is distributed along the lateral direction. This leads to a formation of deformation zone wider along the lateral direction but shallower at the depth for a split specimen configuration. The same can be said for the experimental results of the split specimen, thus it also shows a shallower depth of deformation in contrast to its constrained counterpart.

However, as far as the lateral propagation of the deformation is concerned, both the configurations show an identical character (Fig. 5.10).

Presumably, it can be said due to the severity of the macro-indentation load. Experimentally, split specimen also undergoes a severe plastic deformation and experiences narrower lateral deformation zone in contrast to the simulated findings.

In figure 5.16 and 5.17 the simulated and experimental plastic contours are shown for a constrained specimen configuration. In both cases, the major point of contact beneath the indentation has material homogeneity which aids in propagation of deformation effectively along the vertical direction. Consequently, a higher depth of deformation is observed for a constrained specimen. The plausible cause for this could be the hardening of material beneath the indenter and the same reason can be held accountable for simulation and experimental results too for a constrained specimen. Moreover, in both the configuration, simulation results cannot gauge the experimental results completely. The plausible cause associated to this anomaly could be that in a simulation the analysis does not take the variabilities present due to grain size effect, slip, stacking faults and dislocation defects co-occurring due to severity of the plastic deformation caused by the macro indentation.

7. CONCLUSIONS AND FUTURE SCOPE

- The Sub-surface mapping of hardness values at various locations gives an idea about the extent strain hardening beneath the indenter.

- The values of plastic strains show an exponential decay in both constrained and split specimens. The decay is more in split specimen due the stress release at the interfacial surface in comparison to the constrained specimen.

- For cold work samples the variation in hardness values are not varying significantly, possible reason could be that material has saturated and may behave like an elastic-perfectly plastic material**.**
- The experimental and computational studies conducted beneath a spherical indenter give insights into the deformation zone associated with it. It can be said that the shape of the deformation zone is of elliptical nature.
- The shape of the deformation zone is similar for constrained and bonded interface specimens with only difference being the extent of deformation, which is found to be shallower in vertically down direction along the indenter axis for split specimen in contrast to constrained specimen.
- The simulations cannot assess the experimental results completely which suggests towards the discrepancies in plastic strain distribution.
- As a part of future work, the plastic strain contours can be obtained for the cold work samples by formulating the power law of hardening.
- From simulations perspective, similar study can be performed for cold work samples with considering the plastic properties of the glue layer.

REFERENCES

[1] "www.forgemag.com." .

[2] G. Require- *et al.*, "ASTM E18 − 16 Standard Test Methods for Rockwell Hardness of Metallic Materials," *Am. Soc. Test. Mater.*, pp. 1–38, 2016, doi: 10.1520/E0018-16.

[3] A. G. Atkins and D. Tabor, "Plastic indentation in metals with cones," *J. Mech. Phys. Solids*, vol. 13, no. 3, pp. 149–164, 1965, doi: 10.1016/0022-5096(65)90018-9.

[4] L. E. Samuels and T. O. Mulhearn, "An experimental investigation of the deformed zone associated with indentation hardness impressions," *J. Mech. Phys. Solids*, vol. 5, no. 2, pp. 125–134, 1957, doi: 10.1016/0022-5096(57)90056-X.

[5] T. O. Mulhearn, "The deformation of metals by vickers-type pyramidal indenters," *J. Mech. Phys. Solids*, vol. 7, no. 2, pp. 85–88, 1959, doi: 10.1016/0022-5096(59)90013-4.

[6] K. L. Johnson, "The correlation of indentation experiments," *J. Mech. Phys. Solids*, vol. 18, no. 2, pp. 115–126, 1970, doi: 10.1016/0022-5096(70)90029-3.

[7] M. M. Chaudhri, "Subsurface plastic strain distribution around spherical indentations in metals," *Philos. Mag. A Phys. Condens. Matter, Struct. Defects Mech. Prop.*, vol. 74, no. 5, pp. 1213–1224, 1996, doi: 10.1080/01418619608239721.

[8] K. Eswar Prasad, N. Chollacoop, and U. Ramamurty, "Role of indenter angle on the plastic deformation underneath a sharp indenter and on representative strains: An experimental and numerical study," *Acta Mater.*, vol. 59, no. 11, pp. 4343–4355, 2011, doi: 10.1016/j.actamat.2011.03.058.

[9] H. Helbawi, L. Zhang, and I. Zarudi, "Difference in subsurface damage in indented specimens with and without bonding layer," *Int. J. Mech. Sci.*, vol. 43, no. 4, pp. 1107–1121, 2001, doi: 10.1016/S0020-7403(00)00032-1.

[10] S. Jana, R. Bhowmick, Y. Kawamura, K. Chattopadhyay, and U. Ramamurty, "Deformation morphology underneath the Vickers indent in a Zr-based bulk metallic glass," *Intermetallics*, vol. 12, no. 10-11 SPEC. ISS., pp. 1097–1102, 2004, doi: 10.1016/j.intermet.2004.04.018.

11] H. W. Zhang, G. Subhash, X. N. Jing, L. J. Kecskes, and R. J. Dowding, "Evaluation of hardness-yield strength relationships for bulk metallic glasses," *Philos. Mag. Lett.*, vol. 86, no. 5, pp. 333–345, 2006, doi: 10.1080/09500830600788935.

[12] G. Subhash and H. Zhang, "Dynamic indentation response of ZrHf-based bulk metallic glasses," *J. Mater. Res.*, vol. 22, no. 2, pp. 478–485, 2007, doi: 10.1557/jmr.2007.0058.

[13] J. J. Kruzic, D. K. Kim, K. J. Koester, and R. O. Ritchie, "Indentation techniques for evaluating the fracture toughness of biomaterials and hard tissues," *J. Mech. Behav. Biomed. Mater.*, vol. 2, no. 4, pp. 384–395, 2009, doi: 10.1016/j.jmbbm.2008.10.008.

[14] R. Hill, E. H. Lee, and S. J. Tupper, "The theory of wedge indentation of ductile materials," *Proc. R. Soc. London. Ser. A. Math. Phys. Sci.*, vol. 188, no. 1013, pp. 273–289, 1947, doi: 10.1098/rspa.1947.0009.

[15] D. S. Dugdale, "Vickers hardness and compressive strength," *J. Mech. Phys. Solids*, vol. 6, no. 2, pp. 85–91, 1958, doi: 10.1016/0022-5096(58)90017-6.

[16] D. M. Marsh and P. R. S. L. A, "Plastic flow in glass," *Proc. R. Soc. London. Ser. A. Math. Phys. Sci.*, vol. 279, no. 1378, pp. 420–435, 1964, doi: 10.1098/rspa.1964.0114.

[17] HIRST W and HOWSE MGJW, "Indentation of Materials By Wedges," vol. 311, no. 1506, pp. 429–444, 1969.

[18] A. K. Bhattacharya, J. J. Petrovic, and S. C. Danforth, "Indentation Method for Determining the Macroscopic Fracture Energy of Brittle Bimaterial Interfaces," *J. Am. Ceram. Soc.*, vol. 75, no. 2, pp. 413–417, 1992, doi: 10.1111/j.1151-2916.1992.tb08195.x.

[19] A. E. Giannakopoulos and S. Suresh, "Determination of elastoplastic properties by instrumented sharp indentation," *Scr. Mater.*, vol. 40, no. 10, pp. 1191–1198, 1999, doi: 10.1016/S1359-6462(99)00011-1.

[20] G. Srikant, N. Chollacoop, and U. Ramamurty, "Plastic strain distribution underneath a Vickers Indenter: Role of yield strength and work hardening exponent," *Acta Mater.*, vol. 54, no. 19, pp. 5171–5178, 2006, doi: 10.1016/j.actamat.2006.06.032.

21] U. Ramamurty, S. Jana, Y. Kawamura, and K. Chattopadhyay, “Hardness and plastic deformation in a bulk metallic glass,” *Acta Mater.*, vol. 53, no. 3, pp. 705–717, 2005, doi: 10.1016/j.actamat.2004.10.023.

[22] K. Eswar Prasad and U. Ramamurty, “Effect of temperature on the plastic zone size and the shear band density in a bulk metallic glass,” *Mater. Sci. Eng. A*, vol. 535, pp. 48–52, 2012, doi: 10.1016/j.msea.2011.12.040.

[23] T. G. Murthy, C. Saldana, M. Hudspeth, and R. M’Saoubi, “Deformation field heterogeneity in punch indentation,” *Proc. R. Soc. A Math. Phys. Eng. Sci.*, vol. 470, no. 2166, 2014, doi: 10.1098/rspa.2013.0807.